J. Fluid Mech. (2013), *vol.* 715, *pp.* 1–31.
doi:10.1017/jfm.2012.484

Unsteady feeding and optimal strokes of model ciliates

Sébastien Michelin[1],† **and Eric Lauga**[2]

[1]LadHyX – Département de Mécanique, Ecole polytechnique, 91128 Palaiseau CEDEX, France

[2]Department of Mechanical and Aerospace Engineering, University of California San Diego, 9500 Gilman Drive, La Jolla, CA 92093-0411, USA

(Received 20 June 2012; revised 21 September 2012; accepted 27 September 2012)

The flow field created by swimming micro-organisms not only enables their locomotion but also leads to advective transport of nutrients. In this paper we address analytically and computationally the link between unsteady feeding and unsteady swimming on a model micro-organism, the spherical squirmer, actuating the fluid in a time-periodic manner. We start by performing asymptotic calculations at low Péclet number (Pe) on the advection–diffusion problem for the nutrients. We show that the mean rate of feeding as well as its fluctuations in time depend only on the swimming modes of the squirmer up to order $Pe^{3/2}$, even when no swimming occurs on average, while the influence of non-swimming modes comes in only at order Pe^2. We also show that generically we expect a phase delay between feeding and swimming of 1/8th of a period. Numerical computations for illustrative strokes at finite Pe confirm quantitatively our analytical results linking swimming and feeding. We finally derive, and use, an adjoint-based optimization algorithm to determine the optimal unsteady strokes maximizing feeding rate for a fixed energy budget. The overall optimal feeder is always the optimal steady swimmer. Within the set of time-periodic strokes, the optimal feeding strokes are found to be equivalent to those optimizing periodic swimming for all values of the Péclet number, and correspond to a regularization of the overall steady optimal.

Key words: biological fluid dynamics, low-Reynolds-number flows, micro-organism dynamics

1. Introduction

In order to be able to swim in viscous fluids, micro-organisms must undergo non-time-reversible sequences of shape changes referred to as swimming strokes (Lighthill 1975; Purcell 1977; Lauga & Powers 2009). Through the no-slip boundary condition, these strokes induce a net flow field around the organism and a distribution of viscous stresses which lead to locomotion. This swimming-induced flow also impacts hydrodynamic interactions with neighbouring organisms (Drescher *et al.* 2009; Michelin & Lauga 2010*b*) or material boundaries (Lauga *et al.* 2006; Berke *et al.* 2008), the overall dynamics of suspensions of cells (Kessler 1986; Pedley & Kessler

† Email address for correspondence: sebastien.michelin@ladhyx.polytechnique.fr

1992; Sokolov *et al.* 2007; Saintillan & Shelley 2008*a*; Evans *et al.* 2011) and the feeding ability of organisms (Childress, Koehl & Miksis 1987; Short *et al.* 2006).

Cellular motility is essential to many biological functions, from reproduction (Suarez & Pacey 2006) to escaping aggression (Crawford & Purdie 1992; Hamel *et al.* 2011). It also allows organisms to travel toward better local environments for example to seek (or escape) light, nutrient, or heat. The performance of the particular stroke displayed by a single micro-organism, or that of a suspension of such swimmers, also results in the modification of the bulk stress and effective viscosity of a flow (Batchelor 1970; Ishikawa, Simmonds & Pedley 2007), or of its mixing properties (Saintillan & Shelley 2008*b*; Leptos *et al.* 2009; Kurtuldu *et al.* 2011), an effect that is suspected to play an important role on large-scale bio-mixing in the ocean for example (Doostmohammadi, Stocker & Ardekani 2012).

The metabolism of many micro-organisms relies on the absorption of diffusing nutrients present in their vicinity, ranging from dissolved gases and low-weight proteins, to more complex molecular compounds and, in the case of large organisms such as the protozoon *Paramecium*, smaller bacteria whose run-and-tumble motion is equivalent to a diffusive process at the scale of *Paramecium* (Berg 1993). For a particular micro-organism, the impact of the stroke on its feeding ability can be thought of as twofold: (i) through the motility resulting from the stroke, the organism can travel toward nutrient-rich regions; (ii) by stirring nutrients in its immediate vicinity, the stroke-induced flow modifies, and possibly enhances, local concentration gradients.

The competition of advective and diffusive effects on the dynamics of a particular nutrient is quantified in the Péclet number, $Pe = \tau_{diff}/\tau_{adv}$, where $\tau_{diff} = a^2/\kappa$ and $\tau_{adv} = a/\mathsf{U}$ are the characteristic diffusive and advective time scales respectively, where a, U and κ are the typical size of the organism, the characteristic flow velocity, and the nutrient diffusivity, respectively. Depending on the nutrient considered, Pe can vary by several orders of magnitude, even for a given micro-organism.

Performing its stroke represents an energetic cost for the organism, as it must work against the fluid to overcome viscous dissipation. How far it can swim or how much nutrient it can absorb is therefore, in theory, limited by the finite amount of energy it has available. Considering that energy losses other than hydrodynamic can be accounted for by a fixed metabolic efficiency, the optimization of the swimming stroke to maximize either motility or feeding can therefore be formulated as follows: for a fixed amount of energy available to deform its shape, what is the optimal stroke of a particular micro-organism maximizing either: (i) the net displacement (optimal swimming problem); or (ii) the amount of a particular nutrient absorbed at the surface of the organism (optimal feeding problem)? In the latter case, the optimal stroke does not necessarily require a net displacement of the cell, as the organism can potentially just sit at a given location and stir the fluid around it. The optimal feeding stroke may also depend on the particular nutrient considered and the relative importance of advection and diffusion through the value of Pe.

The optimization problems described above are closely linked to the question of optimality with respect to a specific biological function, which can take two different forms: optimal shape or optimal gait. In the former, one is interested in the optimal morphology of the swimmer (e.g. its aspect ratio, the use of flagella versus cilia, etc.) and compares different species of micro-organisms. In the latter, the focus is placed on a given organism, and the goal is to determine the sequence of body deformations

that performs best (Tam & Hosoi 2007; Spagnolie & Lauga 2010; Michelin & Lauga 2010*a*, 2011; Tam & Hosoi 2011*a*,*b*).

In this work, we focus on the optimal gait of a particular swimmer model, the so-called squirmer. This canonical model, consisting of a spherical micro-organism imposing a tangential velocity at its surface, was introduced as a so-called envelope model for ciliated micro-organisms (Lighthill 1952; Blake 1971). Ciliates, such as *Paramecium*, swim in viscous flows using the coordinated beating of a large number of small cilia distributed over their surface (Blake & Sleigh 1974; Brennen & Winnet 1977). In the squirmer model, the flow field can be determined analytically through the projection of the stroke on orthogonal squirming modes. Because of its simplicity, this model has been used to study a large variety of problems related to swimming micro-organisms, including hydrodynamic interactions (Ishikawa, Simmonds & Pedley 2006), mixing (Lin, Thiffeault & Childress 2011), suspension rheology (Ishikawa & Pedley 2007), collective dynamics and instabilities (Ishikawa *et al.* 2007; Evans *et al.* 2011), and feeding (Magar, Goto & Pedley 2003; Magar & Pedley 2005; Doostmohammadi *et al.* 2012).

Recently, Michelin & Lauga (2010*a*) determined the optimal time-periodic swimming strokes (i.e. those maximizing the swimming velocity for fixed energetic cost) of such a model micro-organism, and identified their main properties. In a subsequent contribution, Michelin & Lauga (2011) considered the optimization of the stroke for feeding in the particular case of a steady surface velocity. Although such strokes correspond to non-periodic displacements of the surface, the results shed some light on the link between swimming and feeding, and in particular it was shown that optimal swimming strokes and optimal feeding strokes were essentially identical regardless of Pe, a result that is not *a priori* intuitive due to the fundamental differences in the impact of swimming on feeding at low or high Pe: at low Pe, swimming only impacts marginally the nutrient distribution, but enables the organism to travel toward regions with richer nutrient content, while at high Pe, swimming also impacts feeding through stirring and strong advection of the nutrient in the vicinity of the organism surface.

The validity of these conclusions, and in particular the intimate relationship between optimal swimming and optimal feeding, remains to be addressed in the general case of unsteady strokes, however. Magar & Pedley (2005) showed that in the particular limit of large Pe and small surface displacement, an equivalent steady problem could be defined. However, the unsteady effects of advection and diffusion in the general case of both finite swimmer displacement and finite Pe remain unclear. In this paper, we specifically focus on the unsteady swimming problem. We first address analytically and computationally the link between unsteady feeding and unsteady swimming. We then derive, and use, an adjoint-based optimization algorithm to determine the optimal unsteady strokes maximizing feeding rate for a fixed energy budget.

The paper is organized as follows. In § 2, the squirmer model is briefly presented, and the swimming and feeding problems are posed mathematically. In § 3, the unsteady feeding rate is determined in the asymptotic limit of small Pe. The impact of the swimming stroke and of the Péclet number on the feeding rate is further analysed in § 4 using numerical simulations, providing an important insight into the link between swimming and feeding. Section 5 presents the result of the stroke optimization with respect to feeding and conclusions and perspectives are finally presented in § 6.

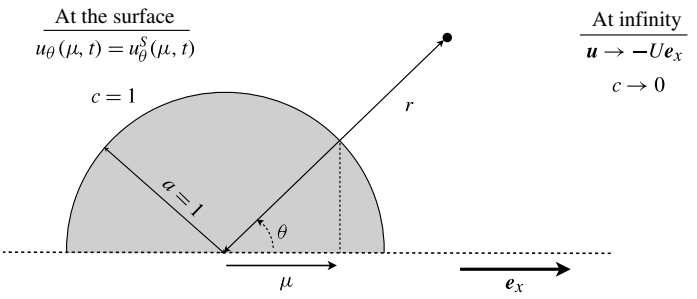

FIGURE 1. Swimming and feeding of a squirmer. A purely axisymmetric tangential velocity and a purely absorbing boundary condition for the nutrient are imposed at the surface of the swimmer. All variables are non-dimensional.

2. Swimming and feeding of a model ciliate

2.1. *The squirmer model*

The present work focuses on a particular model micro-organism, the squirmer, illustrated in figure 1. It is a spherical organism of radius a which prescribes periodic tangential deformations of its surface S with a frequency ω, in order to swim in a viscous fluid of dynamic viscosity μ_f and density ρ_f. The present analysis is restricted to purely axisymmetric deformations of S so that the swimming velocity is parallel to the axis of symmetry $\boldsymbol{e}_x$, with no rotation. In this paper, we will seek optimal strokes maximizing the feeding rate of the organism for a given amount of energy available during each period to perform its surface deformation (and possibly its swimming). This average rate of energy consumption, $\mathscr{P}$, is identified with the rate of work applied on the fluid by the swimmer at its surface, or, equivalently, the total mechanical energy dissipated in the fluid through viscous effects during one period. It is related to the typical surface velocity scale $\mathscr{U}$ by

$$\mathscr{U} = \sqrt{\frac{\mathscr{P}}{12\pi\mu_f a}}. \tag{2.1}$$

The squirmer is swimming in a continuous suspension of a given nutrient (e.g. bacteria, large proteins/molecules, heat, etc.) characterized by a far-field concentration C_∞ and a diffusivity κ, and advected by the flow created by the surface stroke. On the swimmer boundary, the nutrient is instantaneously absorbed and processed at the surface so that $C = C_b$, with C_b the equilibrium concentration at the surface determined by the processing mechanism. A more realistic, but more complex, boundary condition was proposed by Magar *et al.* (2003) and Magar & Pedley (2005), taking into account such effects as the resistance of the membrane to nutrient absorption, and the finite diffusion and processing time of the nutrient within the cell. The instantaneous nutrient uptake by the organism through diffusion at its boundary, $\Phi(t)$, is given by

$$\Phi(t) = \int_{\mathsf{S}} \kappa \frac{\partial C}{\partial r}\, \mathrm{d}S. \tag{2.2}$$

In the case of a purely rigid sphere, with no advection, a steady nutrient flux is achieved through diffusion, $\Phi_0 = 4\pi a\kappa(C_\infty - C_b)$. In the following, we focus on the modification of the concentration field by the organism and define the rescaled concentration field $c = (C_\infty - C)/(C_\infty - C_b)$.

Three distinct time scales are present in the problem: (i) a diffusive time scale $\tau_d = a^2/\kappa$; (ii) an advective time scale $\tau_a = a/\mathscr{U}$; and (iii) the stroke period $\tau_\omega = 2\pi/\omega$. Only the latter two were present in the purely swimming problem (Michelin & Lauga 2010*a*) and only the first two in the steady feeding problem (Michelin & Lauga 2011). The Péclet number, $Pe = \tau_d/\tau_a$, is a measure of the relative importance of advective and diffusive effects near the surface of the squirmer, and is equal to

$$Pe = \frac{\mathscr{U}a}{\kappa} = \frac{1}{\kappa}\sqrt{\frac{\mathscr{P}a}{12\pi\mu_f}}. \tag{2.3}$$

A second independent time scale ratio can be defined either as a characteristic of the stroke, for example the relative velocity $U_R = \mathscr{U}/(a\omega)$, or as a period-based Péclet number $Pe_\omega = a^2\omega/\kappa$. In the following, all equations and quantities are non-dimensionalized using a, ω, μ_f and $C_\infty - C_b$ as reference quantities.

2.1.1. *Swimming problem*

Owing to the small size of the organisms considered, the Reynolds number, $Re = \rho_f\mathscr{U}a/\mu_f$, a relative measure of inertia and viscous effects in the flow, is always much smaller than one, and the velocity and pressure fields satisfy Stokes equations. The swimming problem in the reference frame attached to the organism is therefore

$$\nabla^2\boldsymbol{u} = \boldsymbol{\nabla}p, \quad \boldsymbol{\nabla}\cdot\boldsymbol{u} = 0, \tag{2.4}$$

with the boundary conditions on the swimmer surface and at infinity given by

$$\boldsymbol{u} = u_\theta^S(\mu, t)\boldsymbol{e}_\theta \quad \text{at } r = 1, \tag{2.5}$$

$$\boldsymbol{u} \to -U(t)\boldsymbol{e}_x \quad \text{for } r \to \infty. \tag{2.6}$$

Note that the prescribed surface field, u_θ^S, is the stroke imposed by the organism and at the origin of both locomotion and stirring. The stroke is assumed to be axisymmetric, therefore the surface velocity only depends on $\mu = \cos\theta$ and t, with θ the polar angle measured from the swimming direction $\boldsymbol{e}_x$ (figure 1). In Stokes flow, the swimmer cannot sustain any net hydrodynamic force, therefore we have

$$\int_S [-p\mathbf{1} + (\boldsymbol{\nabla}\boldsymbol{u} + \boldsymbol{\nabla}\boldsymbol{u}^{\mathrm{T}})]\cdot\boldsymbol{n}\,\mathrm{d}S = 0, \tag{2.7}$$

where $\boldsymbol{n}$ is the unit normal vector pointing into the fluid ($\boldsymbol{n} = \boldsymbol{e}_r$ here). Note that we have assumed the swimmer to be neutrally buoyant. The solution to the swimming problem in (2.4)–(2.7) is obtained by decomposing the surface velocity onto the squirming modes (Blake 1971; Michelin & Lauga 2010*a*)

$$u_\theta^S(\mu, t) = \sum_{n=1}^{\infty}\alpha_n(t)K_n(\mu), \tag{2.8}$$

with

$$K_n(\mu) = \frac{2n+1}{n(n+1)}\sqrt{1-\mu^2}L_n'(\mu), \tag{2.9}$$

where $L_n(\mu)$ is the nth-order Legendre polynomial, and $L'(\mu)$ its first derivative. The values of the pressure field and streamfunction are then obtained as

$$p(r,\mu,t) = p_\infty + \sum_{n=2}^{\infty}\alpha_n(t)P_n(r,\mu), \tag{2.10}$$

$$\psi(r,\mu,t) = \sum_{n=1}^{\infty}\alpha_n(t)\Psi_n(r,\mu), \tag{2.11}$$

with

$$P_n(r,\mu) = -\left(\frac{4n^2-1}{n+1}\right)\frac{L_n(\mu)}{r^{n+1}}, \tag{2.12}$$

$$\Psi_n(r,\mu) = \frac{2n+1}{n(n+1)}(1-\mu^2)L_n'(\mu)\psi_n(r), \tag{2.13}$$

$$\psi_1(r) = \frac{1-r^3}{3r}, \quad \psi_n(r) = \frac{1}{2}\left(\frac{1}{r^n} - \frac{1}{r^{n-2}}\right) \quad \text{for } n \geqslant 2. \tag{2.14}$$

In the decomposition above, the first mode is the only one that contributes to the swimming motion (we have $U(t) = \alpha_1(t)$ for all times) and is referred to as the swimming mode, or 'treadmill'. All remaining modes (including the so-called stresslet, $n = 2$, characterizing the modification of the bulk stress by the swimmer) correspond to higher-order singularities in the far-field flow and do not contribute to the swimming motion.

The dimensionless energetic cost, P, is computed as (Michelin & Lauga 2010*a*)

$$\mathsf{P} = \frac{\mathscr{P}}{12\pi\mu_f a^3\omega^2} = \sum_{n=1}^{\infty}\gamma_n\langle\alpha_n^2\rangle, \tag{2.15}$$

with

$$\gamma_1 = 1 \quad \text{and} \quad \gamma_n = \frac{(2n+1)^2}{3n(n+1)} \quad \text{for } n \geqslant 2, \tag{2.16}$$

and is equal to the rate of working of the squirmer on the fluid through its boundary actuation or, equivalently, to the total energy loss through viscous dissipation in the fluid domain. In the following, we define $\langle f\rangle = (1/2\pi)\int_0^{2\pi} f(t)\,\mathrm{d}t$ as the time-averaging operator over one stroke period. With this definition, $\sqrt{\mathsf{P}}$ is the typical non-dimensional surface velocity of the swimmer. Following Lighthill (1975), the stroke swimming efficiency, η (or scaled energy cost), is defined as the ratio of the energetic cost of pulling a rigid sphere with constant velocity $\langle U\rangle$ and the energetic cost of swimming at the same average velocity, obtained here as (Michelin & Lauga 2010*a*):

$$\eta = \frac{\langle U\rangle^2}{2\mathsf{P}} = \frac{\langle\alpha_1\rangle^2}{2\displaystyle\sum_{n=1}^{\infty}\gamma_n\langle\alpha_n^2\rangle}. \tag{2.17}$$

2.1.2. *Feeding problem*

To evaluate the amount of nutrient absorbed at the surface of the organism, the non-dimensional advection–diffusion problem must be solved:

$$\varepsilon\left(\frac{\partial c}{\partial t}+\boldsymbol{u}\cdot\boldsymbol{\nabla} c\right)=\nabla^2 c \quad \text{with } \varepsilon=\frac{Pe}{\sqrt{\mathsf{P}}}, \tag{2.18}$$

together with the far-field behaviour and purely absorbing boundary conditions on the swimmer surface (figure 1)

$$c\to 0 \quad \text{as } r\to\infty, \tag{2.19}$$

$$c=1 \quad \text{for } r=1. \tag{2.20}$$

In (2.18) the parameter $\varepsilon=\omega a^2/\kappa$ can also be understood as the period-based Péclet number. The flow field, $\boldsymbol{u}$, originates from the organism stroke and is obtained from the squirming mode amplitudes, $\alpha_n(t)$, using (2.11), (2.13) and (2.14). The feeding performance of the stroke is evaluated using the ratio $J(t)=\Phi(t)/\Phi_0$ quantifying the net gain in nutrient uptake in comparison with the purely diffusive case ($Pe=0$). The relative nutrient flux, J, is therefore non-dimensional and given by

$$J(t)=-\frac{1}{2}\int_{-1}^{1}\left.\frac{\partial c}{\partial r}\right|_{r=1}\mathrm{d}\mu. \tag{2.21}$$

2.1.3. *Eulerian versus Lagrangian description*

A given periodic stroke, be it swimming or non-swimming, can be mathematically described following two different approaches.

(*a*) By prescribing at each instant, a periodic surface velocity on each point fixed in the swimmer frame, $u_\theta^S(\mu,t)$, or equivalently a set of functions $\{\alpha_n(t)\}_n$. We will refer to this description in the following as the *Eulerian periodic stroke*.

(*b*) By prescribing periodic trajectories, $\xi(\mu_0,t)$, of material surface points labelled by their reference position on the sphere μ_0. We will refer to this description in the following as the *Lagrangian periodic stroke*. The surface velocity and mode amplitudes, $\alpha_n(t)$, can then be obtained from $\xi(\mu_0,t)$ as (Michelin & Lauga 2010*a*)

$$u_\theta(\xi(\mu_0,t),t)=-\frac{1}{\sqrt{1-\xi\,(\mu_0,t)^2}}\frac{\partial\xi}{\partial t}(\mu_0,t), \tag{2.22}$$

$$\alpha_n(t)=\frac{1}{2}\int_{-1}^{1}L_n[\xi(\mu_0,t)]\frac{\partial^2\xi}{\partial\mu_0\partial t}\,\mathrm{d}\mu_0. \tag{2.23}$$

In both descriptions, the flow velocity is periodic and completely determined by the periodic functions $\alpha_n(t)$. However, in the Eulerian formulation, material surface points do not necessarily have periodic trajectories. Indeed, periodic Lagrangian strokes only represent a subset of periodic Eulerian strokes, namely the ones guaranteeing that every surface point comes back to its original position at the end of a full stroke period. Despite its shortcomings regarding the description of material point trajectories, the Eulerian approach has been the most popular for models of swimmers because of its simplicity, and in particular the possibility to consider steady strokes corresponding to steady surface and flow velocities (Ishikawa *et al.* (2006), Short *et al.* (2006), Doostmohammadi *et al.* (2012), Evans *et al.* (2011) to cite only a few).

2.2. *Optimal swimming and optimal feeding*

For a given amount of energy available to perform a periodic stroke, an organism might have different optimal surface motions depending on the biological function of interest: migration (swimming problem) or nutrient uptake (feeding problem). *A priori*, those two objectives should lead to different optimal strokes, if anything because the optimal feeding stroke may depend on nutrient diffusivity through the value of Pe while the swimming problem does not depend on it.

As emphasized earlier, a periodic stroke can be defined in two different ways, either from an Eulerian point of view (periodic flow field) or from a Lagrangian point of view (periodic material displacement). In our recent contributions, we presented the results of the optimal swimming problem (for both Eulerian and Lagrangian strokes) (Michelin & Lauga 2010*a*) and of the optimal feeding problem in the Eulerian steady framework only (Michelin & Lauga 2011). A brief summary of these results is first presented here.

We start by remarking that, for the swimming problem, Eulerian optimal strokes are necessarily steady and each mode, α_n, is independent of time. This is a direct consequence of the absence of history effect in the swimming problem: the swimming velocity and the energetic cost only depend on the instantaneous surface velocity. The optimal Eulerian stroke is then obtained by choosing the surface velocity distribution maximizing instantaneously the efficiency η. From (2.17) we see that the Eulerian optimal swimming stroke is simply obtained by putting all the energy into the swimming mode, namely $\alpha_n(t) = \delta_{n,1}$. The resulting treadmill swimmer, with an efficiency $\eta_{max} = 50\,\%$, is therefore the overall optimal for locomotion (Leshansky *et al.* 2007; Michelin & Lauga 2010*a*).

In the case of the feeding problem, the presence of a time-derivative in the advection–diffusion equation introduces history effects, and the optimal Eulerian feeding stroke is therefore not necessarily steady. Focusing on the simplified problem of steady strokes, Michelin & Lauga (2011) showed using adjoint-based optimization that the optimal steady feeding stroke is essentially the same as the optimal steady swimming stroke, a result which, surprisingly, remains true for all Péclet numbers.

That result was not obvious *a priori*. The value of the mean feeding rate of the organism for a given stroke is a strong function of the diffusivity of the nutrient, whose distribution around the organism is qualitatively different in the diffusive and advective regimes (Magar *et al.* 2003; Michelin & Lauga 2011). The optimal feeding rate, $\langle J \rangle_{opt}$, depends strongly on Pe, but the stroke to achieve this optimal value does not. This result is important biologically as it implies that, for a given organism, a unique optimal stroke maximizes the nutrient uptake regardless of the details of its diffusive transport. For all Pe, and in the steady Eulerian framework, maximizing feeding and maximizing swimming are therefore equivalent problems.

Although simpler conceptually and mathematically, the Eulerian framework is not appropriate to describe periodic deformations of a material surface, such as, for example, the strokes of ciliated cells. To impose periodicity of the surface motion, it is necessary to turn to the Lagrangian approach and to consider the unsteady swimming and feeding problems. Michelin & Lauga (2010*a*) showed numerically that the optimal Lagrangian swimming stroke could be decomposed into two different parts: an effective stroke, dominated by the swimming mode, α_1, and producing a forward velocity, and a recovery stroke during which material points (e.g. cilia tips) are brought back to their original position with front-like dynamics to minimize their (negative) impact on the swimming velocity. This front, or wave, is reminiscent of metachronal waves observed on ciliated organisms (Brennen & Winnet 1977) and

results from a small phase-shift in the motion of neighbouring surface points leading to global symmetry-breaking at the whole-organism level. When the squirmer model is used to represent a ciliate, the cilia length constrains the maximum displacement of the surface and therefore limits the ability of the swimmer not only to approach the optimal Eulerian stroke (treadmill) during the effective stroke but also to reduce the impact of the recovery stroke on the swimming motion. Using a constrained optimization algorithm, the direct relationship between swimming efficiency and surface displacement amplitude was obtained, and Michelin & Lauga (2010*a*) showed that the optimal efficiency of 50 % could be reached asymptotically.

The optimization of the Lagrangian feeding stroke, however, remains at this point an open question; it is the focus of the present paper. The analysis of the nutrient uptake is first addressed analytically at small Pe. The general unsteady feeding problem is then considered numerically before turning to its optimization.

3. Unsteady feeding at low Pe: asymptotics, scalings and optimum

In this section we focus on the feeding problem in the asymptotic limit of dominant diffusion ($Pe \ll 1$). For a given stroke, this is equivalent to the asymptotic analysis of the advection–diffusion problem in the limit $\varepsilon = Pe/\sqrt{\mathsf{P}} \ll 1$.

3.1. *Steady and unsteady boundary layers*

For a steady velocity field, finding the asymptotic expansion of the scalar concentration, c, and surface flux, J, in the limit $\varepsilon \ll 1$ corresponds to a variation on the classical mass transfer problem near a sedimenting sphere (Acrivos & Taylor 1962; Magar *et al.* 2003; Michelin & Lauga 2011). It is based on matching two different solutions for the scalar field c: near the surface of the sphere, diffusive effects are dominant, and advection only appears as higher-order corrections; in the far-field, a balance of both advection and diffusion leads to the proper decay of c.

In the case of an unsteady velocity field, the two terms on the left hand-side of (2.18) do not have the same scaling in the far field. As a result the decay of the concentration field at infinity is not the same whether one considers the time-average of c or its fluctuations around the mean, and a double boundary layer problem must be considered:

(i) in the near field, $r = O(1)$, diffusion dominates and the absorbing boundary condition ($c = 1$) at the surface of the swimmer is satisfied;

(ii) in the unsteady boundary layer (UBL), $R = \varepsilon^{1/2} r = O(1)$, a balance between diffusive effects and rate of change of the local concentration ensures the proper far-field decay for the time-dependent fluctuations of the concentration field $\mathsf{C}(R, \mu, t) = c(r, \mu, t)$;

(iii) in the steady boundary layer (SBL), $\rho = \varepsilon\, r = O(1)$, a balance between advection by the steady velocity field and diffusion ensures the far-field decay of the time-average concentration $\mathscr{C}_0(\rho, \mu) = \langle c \rangle(r, \mu)$.

3.2. *Asymptotic problem formulation*

Decomposing the mode amplitudes, $\alpha_n(t)$, as well as the concentration field, c, and feeding rate, $J(t)$, into their Fourier components, we write

$$\alpha_n(t) = \sum_{p=-\infty}^{\infty} \alpha_{n,p} \mathrm{e}^{\mathrm{i}pt}, \quad c = \sum_{p=-\infty}^{\infty} c_p(r, \mu) \mathrm{e}^{\mathrm{i}pt}, \quad J(t) = \sum_{p=-\infty}^{\infty} J_p \mathrm{e}^{\mathrm{i}pt}. \tag{3.1}$$

The advection–diffusion equation becomes then

$$\text{in the near field,} \quad D\,c_p = \varepsilon\left(\mathrm{i}pc_p + \sum_{n=1}^{\infty}\sum_{q=-\infty}^{\infty}\alpha_{n,q}l_n\,c_{p-q}\right), \tag{3.2}$$

$$\text{in the UBL,} \quad \mathsf{D}\,\mathsf{C}_p = \mathrm{i}p\mathsf{C}_p + \varepsilon^{1/2}\sum_{q=-\infty}^{\infty}\alpha_{1,q}\mathsf{L}_1\,\mathsf{C}_{p-q} + O(\varepsilon^{3/2}), \tag{3.3}$$

$$\text{in the SBL,} \quad \mathscr{D}\,\mathscr{C}_0 = \alpha_{1,0}\,\mathscr{L}_1\,\mathscr{C}_0 + O(\varepsilon^2). \tag{3.4}$$

In (3.2)–(3.4), the following linear operators have been defined

$$D = \frac{1}{r^2}\left[\frac{\partial}{\partial r}\left(r^2\frac{\partial}{\partial r}\right) + \frac{\partial}{\partial\mu}\left((1-\mu^2)\frac{\partial}{\partial\mu}\right)\right], \tag{3.5}$$

$$l_1 = -\left(1-\frac{1}{r^3}\right)\mu\frac{\partial}{\partial r} - \frac{1-\mu^2}{r}\left(1+\frac{1}{2r^3}\right)\frac{\partial}{\partial\mu}, \tag{3.6}$$

$$l_n = \frac{2n+1}{2}\left[\left(\frac{1}{r^{n+2}}-\frac{1}{r^n}\right)L_n(\mu)\frac{\partial}{\partial r} - \frac{(1-\mu^2)L_n'(\mu)}{n(n+1)}\left(\frac{n}{r^{n+3}}-\frac{n-2}{r^{n+1}}\right)\frac{\partial}{\partial\mu}\right], \tag{3.7}$$

$$\mathsf{L}_1 = -\mu\frac{\partial}{\partial R} - \frac{(1-\mu^2)}{R}\frac{\partial}{\partial\mu}, \tag{3.8}$$

and D (respectively $\mathscr{D}$) is identical to D in (3.5) after replacing r by R (respectively ρ), and $\mathscr{L}_1$ is defined as L_1 after replacing R by ρ. The following boundary conditions must also be satisfied:

$$\forall p, \quad c_p(r=1) = \delta_{p,0}, \tag{3.9}$$

$$\forall p \neq 0, \quad \mathsf{C}_p(R\to\infty) = 0, \tag{3.10}$$

$$\mathscr{C}_0(\rho\to\infty) = 0. \tag{3.11}$$

3.3. *Matched asymptotic expansion*

A regular series expansion in $\varepsilon^{1/2}$ of c_p, C_p and $\mathscr{C}_0$ is then performed up to $O(\varepsilon^{3/2})$. We write

$$c_p = \sum_{q=0}^{3}\varepsilon^{q/2}c_p^q + O(\varepsilon^2), \quad \mathsf{C}_p = \sum_{q=0}^{3}\varepsilon^{q/2}\mathsf{C}_p^q + O(\varepsilon^2), \quad \mathscr{C}_0 = \sum_{q=0}^{3}\varepsilon^{q/2}\mathscr{C}_0^q + O(\varepsilon^2). \tag{3.12}$$

At each order, c_p and C_p are to be matched for $r\to\infty$ and $R\to 0$, while C_0 and $\mathscr{C}_0$ are to be matched in the limit $R\to\infty$ and $\rho\to 0$.

Here, the non-homogeneous forcing (3.9) only acts on the steady-state component of the concentration field, and is transmitted to the time-dependent components by advection. Therefore, from the scalings of the different terms in (3.2)–(3.3),

$$\forall p \neq 0, \quad c_p = O(\varepsilon c_0) \quad \text{and} \quad \mathsf{C}_p = O(\varepsilon^{1/2}\mathsf{C}_0). \tag{3.13}$$

3.3.1. $O(1)$

At this order, advection is neglected and the solution is simply the steady diffusive solution $c_p^0 = \delta_{p,0}/r$, which satisfies both near-field and far-field boundary conditions. Therefore, $\mathsf{C}_p^0 = \mathscr{C}_0^0 = 0$ for all p. The resulting feeding rate is

$$J_p = \delta_{p,0} + O(\varepsilon^{1/2}). \tag{3.14}$$

3.3.2. $O(\varepsilon^{1/2})$

Using (3.13), $c_p^1 = 0$ and $\mathsf{C}_p^1 = 0$ for all $p \neq 0$. The steady components c_0^1, C_0^1, and $\mathscr{C}_0$ satisfy

$$D\, c_0^1 = 0, \tag{3.15}$$

$$\mathsf{D}\, \mathsf{C}_0^1 = 0, \tag{3.16}$$

$$\mathscr{D}\, \mathscr{C}_0^1 = \alpha_{1,0} \mathscr{L}_1\, \mathscr{C}_0^1. \tag{3.17}$$

Solving these equations and matching c_p, C_p and $\mathscr{C}_0$ up to $O(\varepsilon^{1/2})$ leads to

$$c_p^1 = 0, \quad \mathsf{C}_p^1 = \frac{\delta_{p,0}}{R}, \quad \mathscr{C}_0^1 = 0, \tag{3.18}$$

and the resulting feeding rate remains unmodified at this order.

3.3.3. $O(\varepsilon)$

Next, the advection–diffusion equation is expanded up to $O(\varepsilon)$ in each region.

(i) *In the near field*, $r = O(1)$:

$$\begin{aligned} D\, c_p^2 &= \sum_{n=1}^{\infty} \alpha_{n,p} l_n\, c_0^0 \\ &= \frac{\mu \alpha_{1,p}}{r^2} \left(1 - \frac{1}{r^3}\right) - \sum_{n=2}^{\infty} \frac{(2n+1)\alpha_{n,p} L_n(\mu)}{2r^2} \left(\frac{1}{r^{n+2}} - \frac{1}{r^n}\right), \end{aligned} \tag{3.19}$$

whose general solution satisfying the near-field boundary condition, $c_p^2(r=1) = 0$, is obtained as

$$\begin{aligned} c_p^2(r, \mu) = \alpha_{1,p}\mu \left(\frac{3}{4r^2} - \frac{1}{2} - \frac{1}{4r^3}\right) + \sum_{n=1}^{\infty} \gamma_{n,p} L_n(\mu) \left(\frac{1}{r^{n+1}} - r^n\right) \\ - \sum_{n=2}^{\infty} \frac{(2n+1)\alpha_{n,p} L_n(\mu)}{4} \left(\frac{1}{(n+1)r^{n+2}} + \frac{1}{nr^n} - \frac{2n+1}{n(n+1)r^{n+1}}\right), \end{aligned} \tag{3.20}$$

where $\gamma_{n,p}$ are constants to be determined after matching with the UBL solution.

(ii) *In the UBL*, $R = O(1)$:

$$\mathsf{D}\, \mathsf{C}_p^2 - \mathrm{i}p \mathsf{C}_p^2 = \alpha_{1,p} \mathsf{L}_1\, \mathsf{C}_0^1 = \frac{\mu \alpha_{1,p}}{R^2}, \tag{3.21}$$

whose general solution compatible with the boundary condition at infinity (for $p \neq 0$) is

$$\mathsf{C}_0^2 = \frac{\gamma'_{0,0}}{R} - \gamma''_{0,0} + \mu \left(\frac{\gamma'_{1,0}}{R^2} - \gamma''_{1,0} R - \frac{\alpha_{1,0}}{2}\right), \tag{3.22}$$

$$\mathsf{C}_p^2 = \frac{\gamma'_{0,p}}{R} \mathrm{e}^{-R\sqrt{\mathrm{i}p}} + \mu \left[\frac{\mathrm{i}\alpha_{1,p}}{pR^2} + \gamma'_{1,p} \left(\frac{1}{R^2} + \frac{\sqrt{\mathrm{i}p}}{R}\right) \mathrm{e}^{-R\sqrt{\mathrm{i}p}}\right] \quad \text{for } p \neq 0. \tag{3.23}$$

(iii) *In the SBL*, $\rho = O(1)$, the general solution of (3.4) is obtained as (Acrivos & Taylor 1962)

$$\mathscr{C}_0^2 = \frac{1}{\rho} \exp\left(-\frac{\alpha_{1,0}(1+\mu)\rho}{2}\right) \sum_{q=0}^{\infty} K_q^2 L_q(\mu) \left(\sum_{m=0}^{q} \frac{(q+m)!}{(\alpha_{1,0}\rho)^m\, m!(q-m)!}\right), \tag{3.24}$$

where the K_q^2 are constants to be determined in the matching process. Matching c_p, C_p and $\mathscr{C}_0$, up to $O(\varepsilon)$ leads to

$$c_p^2 = \frac{\alpha_{1,0}}{2}\left(\frac{1}{r}-1\right)\delta_{p,0} + \mu\alpha_{1,p}\left(-\frac{1}{2}+\frac{3}{4r^2}-\frac{1}{4r^3}\right) - \sum_{n=2}^{\infty}\frac{(2n+1)\alpha_{n,p}L_n(\mu)}{4}\left(\frac{1}{(n+1)r^{n+2}}+\frac{1}{nr^n}-\frac{2n+1}{n(n+1)r^{n+1}}\right), \quad (3.25)$$

$$\mathsf{C}_0^2 = -\frac{\alpha_{1,0}(1+\mu)}{2}, \quad \mathsf{C}_p^2 = \frac{\mathrm{i}\alpha_{1,p}\mu}{pR^2}[1-(1+R\sqrt{\mathrm{i}p})\mathrm{e}^{-R\sqrt{\mathrm{i}p}}] \quad \text{for } p\neq 0, \quad (3.26)$$

$$\mathscr{C}_0^2 = \frac{1}{\rho}\exp\left(-\frac{\alpha_{1,0}(1+\mu)\rho}{2}\right), \quad (3.27)$$

and the resulting feeding rate expansion is

$$J_p = \delta_{p,0}\left(1+\frac{\varepsilon\alpha_{1,0}}{2}\right)+O(\varepsilon^{3/2}). \quad (3.28)$$

Up to this order, we see that the results of the classical low-*Pe* asymptotic expansion for a steady velocity field are recovered and the mean feeding rate only depends on the average swimming velocity. In order to capture the leading-order unsteady contribution to the feeding problem, the expansion must be carried out to the next order.

3.3.4. $O(\varepsilon^{3/2})$

From (2.21), we see that only the computation of the azimuthal average, $\tilde{c}_p^3$, of the pth Fourier component of the concentration field

$$\tilde{c}_p^3(r) = \frac{1}{2}\int_{-1}^{1} c_p^3(r,\mu)\,\mathrm{d}\mu, \quad (3.29)$$

is necessary in order to compute the $O(\varepsilon^{3/2})$ correction to the nutrient uptake.

(i) *In the near field*, taking the azimuthal average of (3.2) and using (3.18), we have

$$\frac{1}{r^2}\frac{\mathrm{d}}{\mathrm{d}r}\left(r^2\frac{\mathrm{d}\tilde{c}_p^3}{\mathrm{d}r}\right)=0, \quad (3.30)$$

whose general solution satisfying the boundary condition on the sphere is $\tilde{c}_p^3 = a_p(1-1/r)$, where a_p is a constant to be determined by matching with the UBL solution.

(ii) *In the UBL*, taking the azimuthal average of (3.3) and using (3.26), we get

$$\frac{1}{R^2}\frac{\mathrm{d}}{\mathrm{d}R}\left(R^2\frac{\mathrm{d}\tilde{\mathsf{C}}_p^3}{\mathrm{d}R}\right)-\mathrm{i}p\tilde{\mathsf{C}}_p^3 = \frac{1}{2}\sum_{q=-\infty}^{\infty}\alpha_{1,p-q}\int_{-1}^{1}\mathsf{L}_1\,\mathsf{C}_p^2\,\mathrm{d}\mu = \frac{1}{3R}\sum_{q=-\infty}^{\infty}\alpha_{1,p-q}\alpha_{1,q}\mathrm{e}^{-R\sqrt{\mathrm{i}q}}. \quad (3.31)$$

This equation can be solved explicitly for $\tilde{C}_p^3$ using the far-field boundary condition for the non-constant Fourier components and we get

$$\tilde{\mathsf{C}}_0^3 = \frac{\alpha_{1,0}^2 R}{6}+\frac{\tilde{a}_0}{R}+\tilde{b}_0-\sum_{m=1}^{\infty}\frac{2\,|\alpha_{1,m}|^2}{3mR}\mathrm{e}^{-R\sqrt{m/2}}\sin\left(R\sqrt{\frac{m}{2}}\right), \quad (3.32)$$

$$\tilde{\mathsf{C}}_p^3 = \frac{\tilde{a}_p}{R}\mathrm{e}^{-R\sqrt{\mathrm{i}p}} + \frac{\alpha_{1,0}\alpha_{1,p}}{3}\left(\frac{\mathrm{i}}{pR} - \frac{\mathrm{e}^{-R\sqrt{\mathrm{i}p}}}{2\sqrt{\mathrm{i}p}}\right) + \sum_{m=1}^{p-1}\left(\frac{\mathrm{i}\alpha_{1,m}\alpha_{1,p-m}}{3mR}\right)\mathrm{e}^{-R\sqrt{\mathrm{i}(p-m)}} + \sum_{m=p+1}^{\infty}\left(\frac{\mathrm{i}\alpha_{1,m}\overline{\alpha_{1,m-p}}}{3R}\right)\left(\frac{\mathrm{e}^{-R\sqrt{\mathrm{i}(p-m)}}}{m} + \frac{\mathrm{e}^{-R\sqrt{\mathrm{i}m}}}{p-m}\right) \quad \text{for } p \geqslant 1, \tag{3.33}$$

with $\tilde{\mathsf{C}}_p^3$ defined for $p \leqslant -1$ using $\tilde{\mathsf{C}}_{-p} = \overline{\tilde{\mathsf{C}}_p}$.

(iii) *In the SBL*, the equation for $\mathscr{C}_0^3$ is identical to that at the previous order and the general solution takes the same form, see (3.24).

By matching $\tilde{c}_p$, $\tilde{\mathsf{C}}_p$ and $\tilde{\mathscr{C}}_0$ up to $O(\varepsilon^{3/2})$, the values of $\tilde{b}_0$, $\tilde{a}_p$ and a_p can then be determined, and one obtains

$$\langle J\rangle = 1 + \frac{\varepsilon\alpha_{1,0}}{2} + \varepsilon^{3/2}\frac{\sqrt{2}}{3}\sum_{m=1}^{\infty}\frac{|\alpha_{1,m}|^2}{\sqrt{m}} + O(\varepsilon^2), \tag{3.34}$$

$$J(t) - \langle J\rangle = \varepsilon^{3/2}(-\mathrm{i}\sqrt{\mathrm{i}})\sum_{p\neq 0}\tilde{J}_p\mathrm{e}^{\mathrm{i}pt} + O(\varepsilon^2), \tag{3.35}$$

with

$$\tilde{J}_p = \left[\frac{\alpha_{1,0}\alpha_{1,p}}{2\sqrt{p}} + \sum_{m=1}^{p-1}\frac{\alpha_{1,m}\alpha_{1,p-m}}{3m}\left(\sqrt{p} - \sqrt{p-m}\right) + \sum_{m\geqslant p+1}\frac{\alpha_{1,m}\overline{\alpha_{1,m-p}}}{3m(m-p)}\left(m^{3/2} - p^{3/2} - \mathrm{i}\,(m-p)^{3/2}\right)\right]. \tag{3.36}$$

For a given stroke, the limit $\varepsilon \ll 1$ is equivalent to $Pe \ll 1$ and the asymptotic expansion in terms of the Péclet number, Pe, can be obtained by substitution of $\varepsilon = Pe/\sqrt{\mathsf{P}}$ in (3.34)–(3.36).

3.4. *Discussion*

The asymptotic analysis obtained in (3.34)–(3.36) provides some important physical insight into the relationship between the swimming motion and the nutrient uptake on the surface of the swimmer. As for the steady case, the leading-order advective correction to the feeding rate is linear in Pe and only depends on the average velocity of the organism (Acrivos & Taylor 1962; Magar *et al.* 2003). At this order in Pe, there is a direct correlation between swimming and feeding and only the mean feeding rate is modified, fluctuations in time being negligible (higher order).

The next-order correction marks a fundamental difference between the steady and unsteady problems: in the steady case, all squirming modes contribute to the next correction at order Pe^2 (Michelin & Lauga 2011). Instead, in the unsteady feeding problem, a new correction to $J(t)$ (both its mean value in time and fluctuations) appears at order $Pe^{3/2}$, which depends solely on the swimming velocity of the organism (through all the Fourier components, $\alpha_{1,m}$, of the swimming velocity, $\alpha_1(t)$, with no other squirming modes), and dominates the contribution of non-swimming modes that will only enter at $O(Pe^2)$. For all time-periodic strokes, the instantaneous feeding rate is therefore completely determined up to $O(Pe^{3/2})$ by the characteristics of the swimming velocity of the organism.

This result has a major consequence for strokes that swim instantaneously ($U(t) \neq 0$) but do not swim on average ($\langle U\rangle = 0$). In this case, the leading-order improvement

to the feeding rate is solely governed by the zero-mean fluctuations of $U(t)$. Non-swimming modes only contribute to higher-order corrections, even if they have non-zero time averages. Consequently, for an organism that does not have a net swimming motion (e.g. a time-reversible swimmer), an instantaneous zero-mean swimming motion still presents a feeding advantage over stirring strokes where the cell stays in the same position at each instant ($U(t) = 0$).

Our asymptotic expansion also provides some information on the relative phase of swimming and feeding. For an unsteady swimming velocity, $U(t)$, with a single dominant Fourier component, the instantaneous feeding rate has a $\pi/4$ delay on the swimming velocity (since $-\mathrm{i}\sqrt{\mathrm{i}} = \mathrm{e}^{-\mathrm{i}\pi/4}$ in (3.35)). A maximum in the feeding rate is therefore expected to take place after the peak swimming velocity, with a delay of $1/8$th of a period.

Note that the total nutrient flux is fully determined by the body velocity $U(t)$ up to $O(Pe^{3/2})$. Whether the organism is swimming (force-free) or is an actuated rigid sphere (forced motion) does not actually come into play here. All the conclusions above are therefore valid for non-buoyant swimmers, but also for oscillating rigid spheres in Stokes flow, for which the present results represent a generalization of classical steady mass transfer results (Acrivos & Taylor 1962) to unsteady motions (see appendix A for more details).

In summary, our analytical results show that for low Pe, feeding is completely determined by swimming for any periodic stroke. Optimization of the feeding rate for a fixed amount of available energy is therefore equivalent in this limit to maximizing the swimming velocity under the same constraint, namely the swimming efficiency optimization problem. At low Péclet number, the Lagrangian optimal swimming and optimal feeding strokes are therefore identical, which confirms the result obtained in the steady framework by Michelin & Lauga (2011). In addition, similarly to the result for swimming, we get the result that at low Péclet number the optimal unsteady feeding problem is actually steady. This can be seen from (3.34) where the steady Fourier mode, $\alpha_{1,0}$, carries a higher weight than the other Fourier components compared to their relative importance in the rate of working.

4. Unsteady feeding at finite Pe: simulations

To confirm the low-Pe results obtained analytically, we now turn to characterizing the feeding performance of different strokes for intermediate and large Pe. Eulerian periodic strokes are determined by prescribing $\alpha_n(t)$ for all n, while Lagrangian periodic strokes are described by giving the trajectories of material points $\theta = \vartheta(\theta_0, t)$ where θ is the current position of the material point and θ_0 its mean position. Alternatively, those strokes will be defined by $\mu = \xi(\mu_0, t)$, with $\mu = \cos\theta$. For illustration we consider three particular swimming and non-swimming Lagrangian periodic strokes.

(*a*) *Stroke A* is the numerical optimal swimmer identified in Michelin & Lauga (2010*a*) which has swimming efficiency $\eta \approx 20\,\%$.

(*b*) *Stroke B* is a less efficient swimmer obtained using surface deformations in the form of a simple progressive wave:

$$\xi(\mu_0, t) = \mu_0 + A(1 - \mu_0^2)\cos(k\mu_0 - t), \tag{4.1}$$

with $A = 1/3$ and $k = 1$.

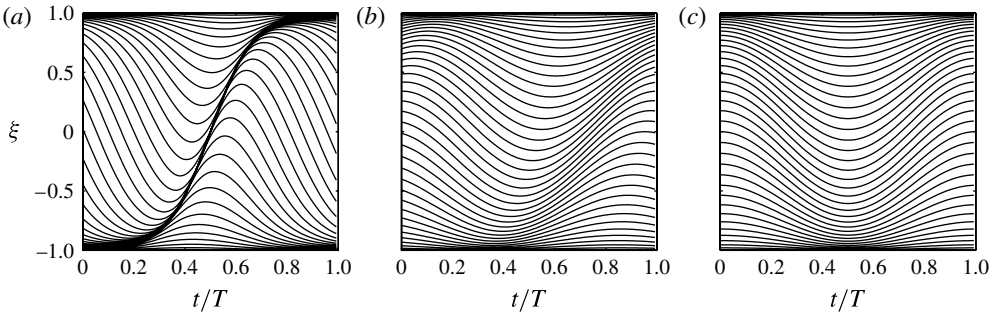

FIGURE 2. Trajectories, $\xi(t)$, of surface material points for stroke A (*a*), stroke B (*b*), and stroke C (*c*). The corresponding time-averaged swimming velocity, $\langle U\rangle$, is equal to 0.33, 0.03 and 0 respectively. The swimming and feeding performances of the three strokes are summarized in table 1.

(*c*) *Stroke C* takes the same form as stroke B but with $A = 1/3$ and $k = 0$. Stroke C represents a time-reversible (or 'reciprocal') deformation, and therefore has no net swimming motion, $\langle U\rangle = 0$.

All three strokes display non-zero instantaneous swimming, but only strokes A and B show swimming on average. Stroke C thus differs from purely stirring strokes for which the organism is strictly still at each instant. The trajectories of material surface points are shown for strokes A, B and C in figure 2. Mathematically, from the knowledge of $\xi(\mu_0, t)$, the mode amplitudes $\alpha_n(t)$ are obtained using (2.23).

4.1. *Numerical solution of the advection–diffusion problem*

For a given set of mode amplitudes, $\{\alpha_n(t)\}$, the advection–diffusion equation (2.18) is solved spectrally in time for each azimuthal component of the concentration field

$$c(r,\mu,t) = \sum_{p=0}^{\infty} c_p^*(r,t)L_p(\mu) = \sum_{k=-\infty}^{\infty}\sum_{p=0}^{\infty} c_p^k(r)L_p(\mu)\mathrm{e}^{\mathrm{i}kt}. \tag{4.2}$$

The functions $c_p^k(r)$ therefore satisfy the following systems of ordinary differential equations for $p \geqslant 0$ and $-\infty < k < \infty$:

$$\left[\frac{1}{Pe}\left(\frac{\mathrm{d}^2}{\mathrm{d}r^2} + \frac{2}{r}\frac{\mathrm{d}}{\mathrm{d}r} - \frac{p(p+1)}{r^2}\right) - \mathrm{i}k\right] c_p^k$$
$$= \sum_{m=0}^{\infty}\sum_{n=1}^{\infty}\sum_{l=-\infty}^{\infty} \frac{\alpha_n^{k-l}}{r^2}\left(A_{mnp}\psi_n\frac{\mathrm{d}}{\mathrm{d}r} + B_{mnp}\frac{\mathrm{d}\psi_n}{\mathrm{d}r}\right) c_m^l, \tag{4.3}$$

with boundary conditions

$$c_p^k(r=1) = \delta_{p,0}\delta_{k,0}, \tag{4.4}$$

$$c_p^k(r\to\infty) = 0. \tag{4.5}$$

In (4.3), A_{mnp} and B_{mnp} are third-order scalar tensors defined in appendix B. Equations (4.3)–(4.5) are discretized on an exponentially-stretched grid in r to concentrate points near the surface of the swimmer (see Michelin & Lauga 2011, for more details), and the solution $\{c_p^k(r_j)\}_{(j,k,p)}$ is then found iteratively. In typical

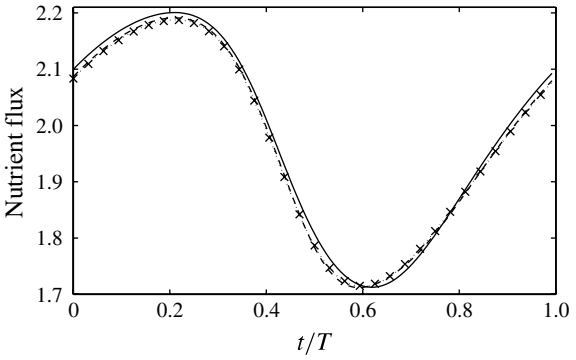

FIGURE 3. Instantaneous nutrient flux at $Pe = 5$ for the optimal swimmer (stroke A) using an increasing number of squirming modes to numerically describe the stroke in the advection–diffusion solver: $n_\alpha = 1$ (solid), $n_\alpha = 2$ (dashed), $n_\alpha = 4$ (dotted) and $n_\alpha = 8$ (crosses). The error made on the average nutrient flux over a period is respectively 0.5 %, 0.03 %, 0.01 % and 0.002 %.

simulations, the resolution used was $N_r = 120$ points for the r-grid, $N_\mu = 40$–100 Legendre polynomials for the azimuthal dependence, $N_t = 16$–128 points in time, and $N_\alpha = 2$–10 squirming modes to describe the swimming stroke.

Alternatively, the advection–diffusion equation can be marched in time for each azimuthal component, $c_p^*(r, t)$, using an explicit time-stepping scheme for the advective terms and Crank–Nicholson for the diffusion term. In the following, the advection–diffusion equation is solved spectrally in time except for strokes that do not swim on average (e.g. stroke C) for which the iterative algorithm does not converge properly or fast enough, and the time-marching approach is used in that case.

Computationally, it is observed that the instantaneous nutrient flux converges rapidly with the number of squirming modes used to represent the swimming stroke, as shown in figure 3. The convergence is even faster for the average nutrient flux: describing stroke A with only the first two squirming modes significantly speeds up the computations while introducing an error smaller than 0.05 % on the average feeding rate. Similar numerical tests performed on less efficient swimmers than stroke A (that is, swimming strokes for which mode 1 is not dominant) did not modify this observation significantly, and restricting the computation to only 2 or 3 squirming modes typically introduces an error smaller than 0.2 %. This rapid convergence of the mean and fluctuating feeding rate is yet another indication that the swimming motion controls the feeding ability of the organism and higher-order modes only act as a small correction to the average feeding rate.

4.2. *Impact of the swimming stroke on the feeding performance*

Figures 4 and 5 show the concentration field around the squirmer for five successive and equispaced instants of a full period, for $Pe = 5$ (figure 4) and $Pe = 30$ (figure 5), and for the three different strokes. For strokes A and B, at lower Péclet number, the nutrient concentration field only shows a weak front–back anisotropy as diffusion dominates over advection, confirming the observations on steady strokes of Magar *et al.* (2003) and Michelin & Lauga (2011). As Pe is increased, sharper concentration gradients can be seen on the front of the squirmer. This results in an increased average feeding rate for increasing Pe as was observed for steady strokes (Michelin & Lauga

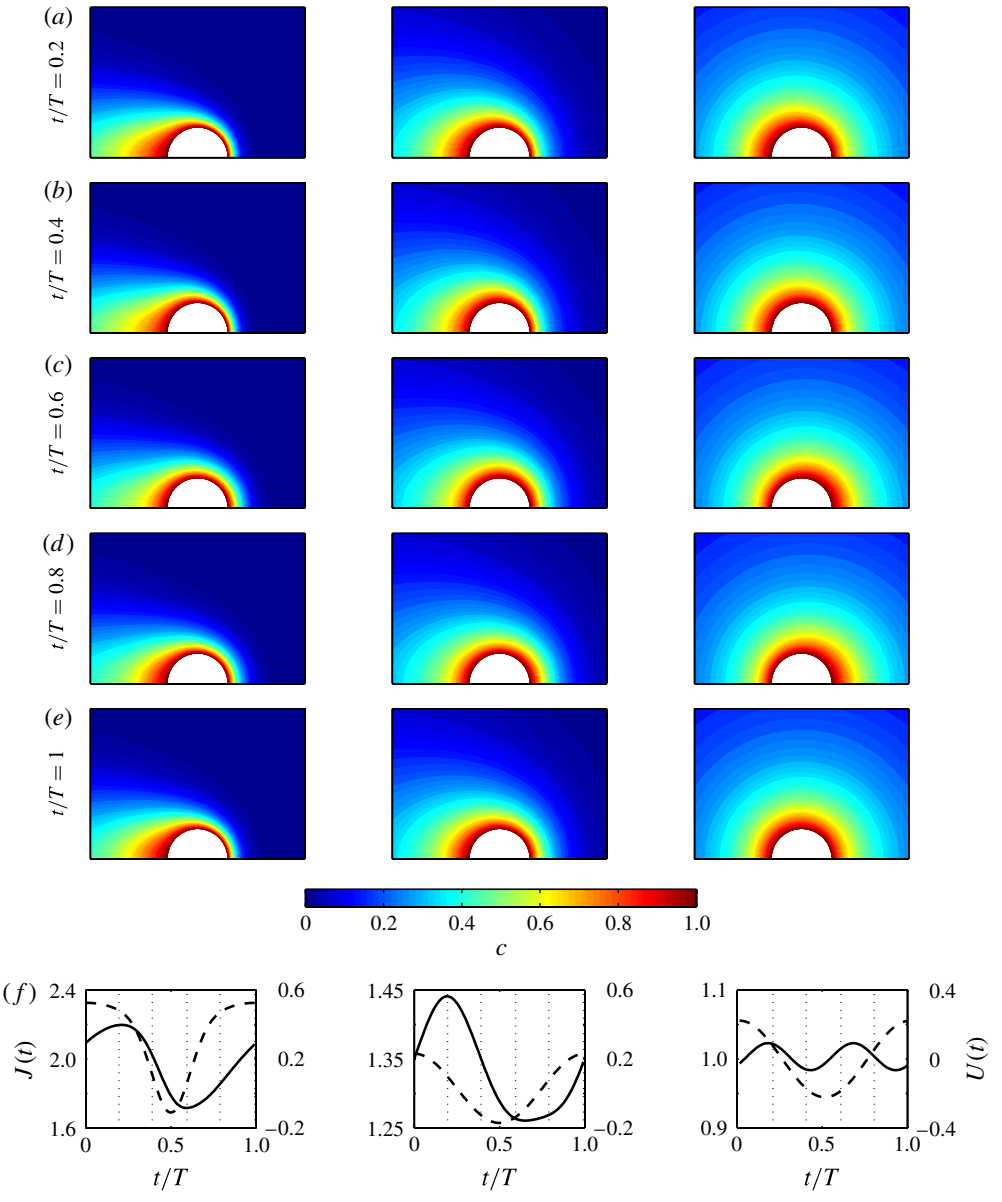

FIGURE 4. (*a–e*) Nutrient concentration around the organism at $Pe = 5$ for stroke A (left), stroke B (middle) and stroke C (right). (*f*) Evolution in time of the feeding rate (solid) and swimming velocity (dashed) for strokes A, B and C (left to right); the dotted lines indicate the time corresponding to each of the five snapshots above.

2011). The main difference with the steady results is that in the unsteady scenario, the velocity of the squirmer changes (and possibly reverses sign) inducing a fluctuation in this front–back anisotropy and in the boundary layer thickness. For stroke C, which does not swim on average, the nutrient concentration field shows a strong isotropy, even at larger *Pe*, with much weaker concentration gradients resulting in a very weak modification of the nutrient uptake $\langle J \rangle$.

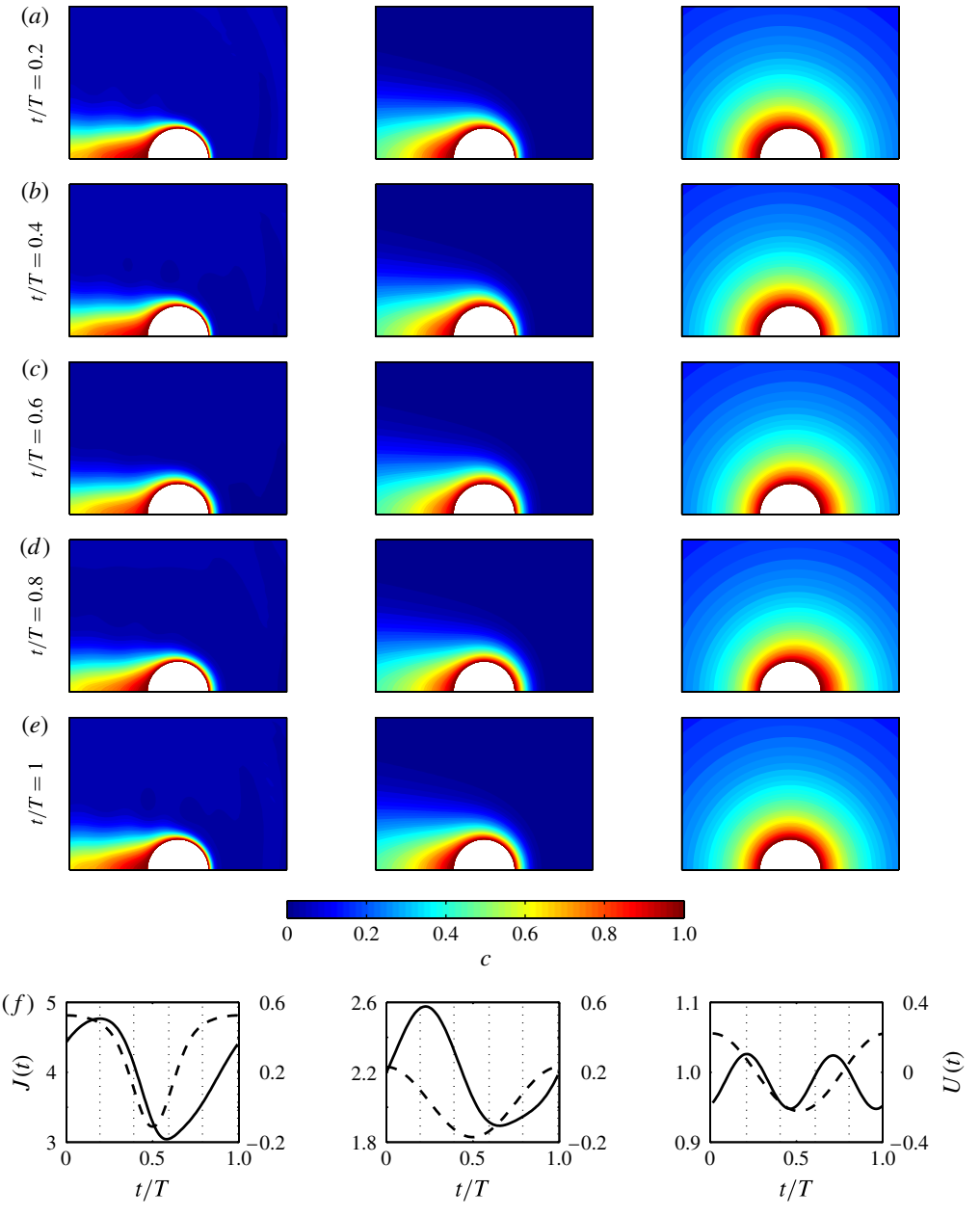

FIGURE 5. Same as figure 4 but with $Pe = 30$.

Comparing the results obtained for the different strokes in table 1, we see that stroke A is clearly more efficient than strokes B and C from a feeding point of view, and stroke A also corresponds to a 'better' swimmer. This is consistent with the increase of the feeding rate with the instantaneous swimming velocity that enables the formation of sharp concentration gradients in front of the squirmer. For stroke C, the periodic reversal of the swimming velocity over the period, and the absence of net displacement, results in the impossibility of maintaining sharp concentration gradients

Stroke	$\langle U \rangle$	η (%)	$\langle J \rangle (Pe = 5)$	$\langle J \rangle (Pe = 30)$
A	0.33	22	1.97	3.98
B	0.030	1.3	1.33	2.19
C	0	0	1.00	0.99

TABLE 1. Swimming and feeding performance of strokes A, B and C.

at the front of the body and of swimming toward regions with richer nutrient content, reducing its feeding ability significantly.

Looking at the temporal variations of the swimming velocity and feeding rate throughout the stroke period (figures 4*f*, 5*f*), a phase delay between the former and the latter is clearly identified for strokes A and B, and for all Pe considered. For stroke C, a similar delay is observed between the peaks in velocity magnitude (positive or negative) and the peaks in feeding rate: for this stroke, the feeding rate frequency is twice that of the swimming velocity because of the exact symmetry between the two half-strokes. The presence of this time delay in all strokes is consistent with the results of the low-Pe asymptotic analysis in § 3 and can be interpreted as the time necessary for the concentration gradient (and possibly boundary layer) to re-establish at the front of the cell when its velocity starts increasing again.

4.3. *Impact of the Péclet number on the feeding performance*

It was observed previously that the value of Pe plays an important role in the feeding ability of the cell. This is investigated further here by looking at the impact of Pe on the instantaneous feeding rate for strokes A, B and C. The instantaneous feeding rate, $J(t)$, is decomposed into its mean value $\langle J \rangle$, the amplitude of its fluctuations in time J_1, and its normalized profile $\tilde{J}(t)$, so we write

$$J(t) = \langle J \rangle + J_1 \tilde{J}(t), \tag{4.6}$$

where $J_1 = \max(J) - \min(J)$ and $\tilde{J}(t) = (J(t) - \langle J \rangle)/J_1$. Similar quantities are also defined for the swimming velocity: $\langle U \rangle$, U_1 and $\tilde{U}$. For a given stroke (A, B or C), the variation of these three quantities with Pe is displayed in figure 6.

For swimming strokes, it is observed that, for low Pe, the modification in the mean feeding rate, $\langle J \rangle - 1$, scales linearly with Pe (strokes A and B). This is consistent with the asymptotic analysis of § 3 and with the steady results in Michelin & Lauga (2011). In such a diffusion-dominated regime, swimming enables the cell to sweep a region of fresher nutrients with an effective cross-section radius that is independent of the swimming velocity (because of the predominance of diffusion) and of the order of the size of the cell. At higher Pe, the reduced importance of diffusion over advection reduces the effective cross-section radius and $\langle J \rangle$ increases at a lower rate with Pe. For strokes with no net swimming motion (stroke C), the modification in the mean feeding rate scales as a higher power, $Pe^{3/2}$, for $Pe \leqslant 0.1$, consistently with the results of the asymptotic analysis.

For both swimming and non-swimming strokes, the amplitude of the feeding rate fluctuations, J_1, varies as $Pe^{3/2}$ for $Pe \leqslant 1$, consistently with our asymptotic results. On figure 6 the fluctuations profile, $\tilde{J}(t)$, is also represented and compared to the leading-order prediction of the asymptotic analysis. We see a very good agreement at low Pe which persists even at high Pe for efficient swimming strokes such as stroke A. This confirms that the feeding rate (both its mean value and its fluctuations) is

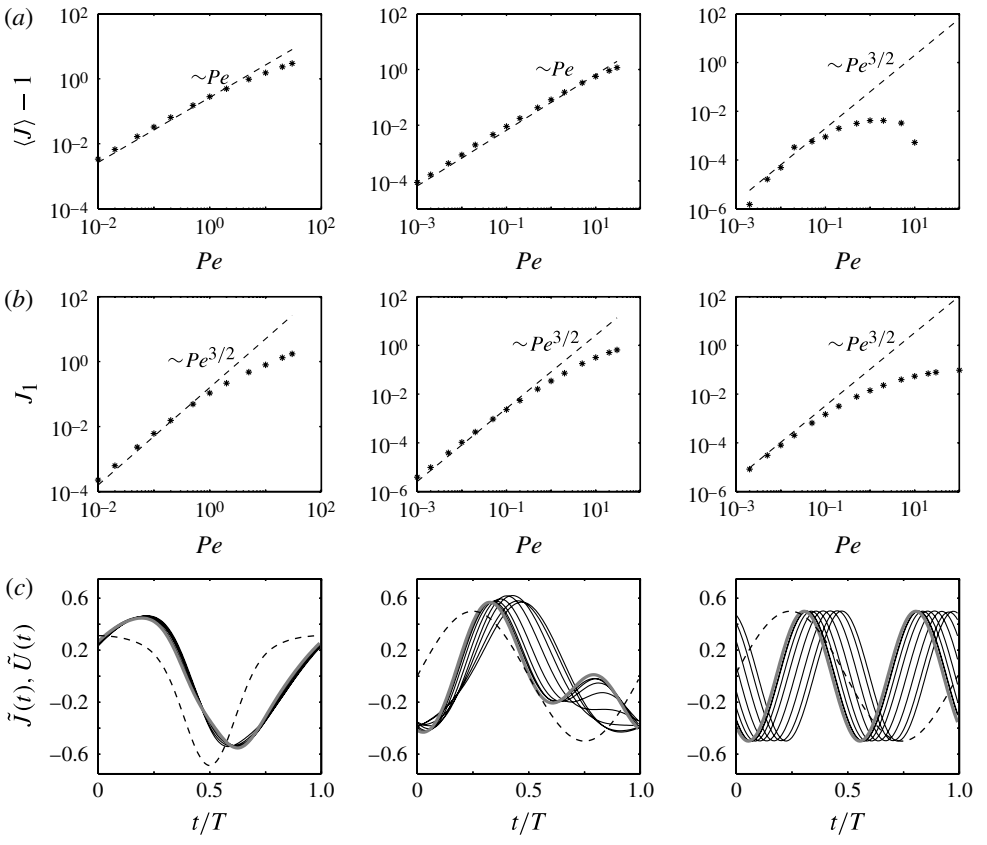

FIGURE 6. (*a*) Dependence of the mean feeding rate, $\langle J\rangle$ (stars), on Pe and comparison with the asymptotic prediction in (3.34) (dashed). (*b*) Dependence of the peak-to-peak amplitude of the feeding rate fluctuations, J_1 (stars), on Pe and comparison with the asymptotic prediction in (3.35)–(3.36). (*c*) Rescaled (unit amplitude) feeding rate (solid) and velocity (dashed) time fluctuations; the asymptotic prediction for the feeding rate fluctuations at low Pe in (3.35)–(3.36) is shown as a thick grey line. All results are plotted for stroke A (left), stroke B (middle), and stroke C (right).

determined at leading order by the swimming mode and corrections from the other modes only play marginal roles. Again, a clear phase delay between the swimming velocity and feeding rate is observed for all Pe, and for the least efficient swimmers considered (B and C), this delay seems to increase with Pe.

When Pe becomes large, another significant difference appears between strokes with zero (stroke C) or non-zero (strokes A and B) mean swimming velocity. For strokes A and B, the average feeding rate continues to increase with Pe, albeit more slowly. From the large-Pe steady results in Michelin & Lauga (2011), we expect $\langle J\rangle$ to scale as $Pe^{1/2}$, when the increase in feeding rate with swimming is driven by the concentration boundary layer thickness around the cell. In contrast, for non-swimming strokes, $\langle J\rangle$ reaches a maximum for a finite value of Pe ($Pe_{c1} \approx 2$) beyond which an increase in Pe actually results in a decrease of the feeding rate. Moreover, beyond a second critical value ($Pe_{c2} \approx 11$ for this particular stroke), the mean feeding rate falls below 1, and for large Pe, swimming actually penalizes feeding as it reduces the net

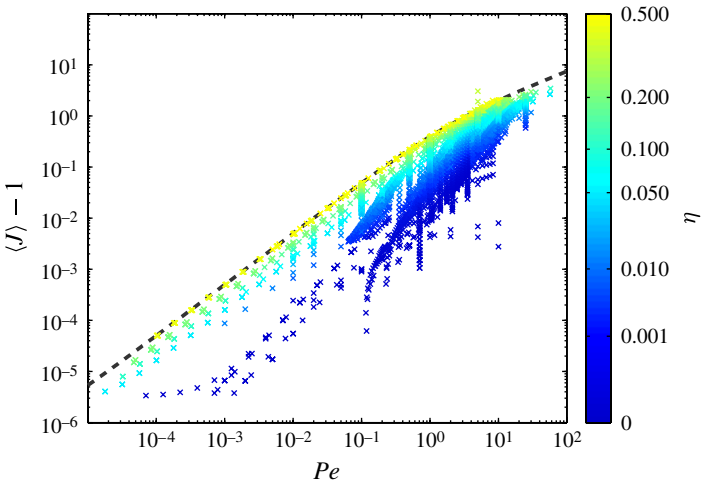

FIGURE 7. (Colour online) Mean feeding rate as a function Pe for 8500 different swimming strokes (see text). The dashed line corresponds to the optimal steady feeding stroke (treadmill). For each stroke, the symbol shade is related to its hydrodynamic efficiency, η.

feeding rate below the level of the purely diffusive regime ($Pe = 0$). This somewhat surprising result can be understood as follows. In stroke C, the sphere swims forward during half of a period leaving behind it a nutrient-depleted wake. In the second half of the stroke, the cell swims backward into this region of poor nutrient concentration, resulting in a reduced flux at the boundary.

4.4. *The optimal unsteady stroke is steady*

As we discussed above, the optimal Eulerian swimming stroke is necessarily steady. The same conclusion cannot be drawn *a priori* for the feeding problem owing to the time-dependence of the advection–diffusion equation (see § 2.2). We saw however that it was true analytically at low Péclet number. Numerically, it also seems to hold as illustrated in figure 7. We performed numerical simulations on a large collection of unsteady Eulerian periodic and Lagrangian periodic strokes (8500 in total), ranging from very efficient to poor swimmers. For all values of Pe, the feeding rate is seen to be always less than that obtained with the optimal steady feeding stroke (treadmill). As for the optimal swimming stroke, the optimal Eulerian unsteady feeding stroke must therefore also be steady. Furthermore, figure 7 demonstrates that the more efficient the unsteady stroke is for swimming, the closer it can get to the optimal feeding rate.

4.5. *Feeding and swimming*

In the previous sections, a relationship between the swimming velocity and the feeding rate was clearly identified, suggesting that at leading order the mean feeding rate is determined by the swimming velocity and Pe. More precisely, and in the light of the steady results of Michelin & Lauga (2011), one expects the feeding rate to be determined by the 'swimming Péclet number', Pe_U, defined as

$$Pe_U = \frac{a\langle U \rangle}{\kappa} = Pe\sqrt{2\eta}, \tag{4.7}$$

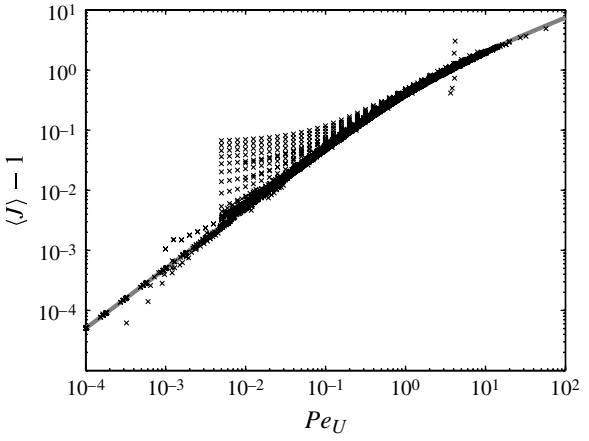

FIGURE 8. Mean feeding rate as a function of the swimming Péclet number $Pe_U = Pe\sqrt{2\eta}$ for the same 8500 strokes as in figure 7. The grey line corresponds to the feeding performance of the steady treadmill swimmer for which $\alpha_n(t) = \delta_{n,1}$.

which measures the relative importance of advection of nutrients by the net displacement of the cell and diffusion. This is clearly the case at leading order for low Pe, as seen in (3.34).

In order to test the validity of this conjecture at higher Pe, we plot in figure 8 the mean feeding rate as a function of the swimming Péclet number Pe_U, for the same large collection of unsteady strokes as in the previous section. All data points collapse rather well on a single curve, that corresponds exactly to the results for the steady treadmill swimmer (Michelin & Lauga 2011). The agreement is particularly good for larger Pe_U, corresponding to more efficient swimming strokes where the swimming motion dominates. The collapse of all the data points on that curve indicates that at leading order, for all strokes and all Pe, the mean feeding rate is determined by the mean swimming velocity.

Figure 8 shows however that a significant number of points do not follow that leading-order trend and are located above the grey treadmill curve. Indeed, for swimming strokes with poor efficiency (including those with $Pe_U = 0$), the contribution from the mean swimming velocity to the mean feeding process is no longer dominant and the influence of other squirming modes, or from time variations of the swimming velocity, cannot be neglected, so $\langle J \rangle$ remains strictly greater than one.

5. Optimal unsteady feeding

The results presented in the previous sections and in Michelin & Lauga (2011) suggest that: (i) swimming determines feeding, at least at leading order, and as a result (ii) optimal swimming and optimal feeding strokes are essentially identical. In this section result (ii) is confirmed directly by performing an optimization of the swimming stroke maximizing the average nutrient uptake for a fixed energetic cost. The approach and methods presented below are based on the frameworks presented in Michelin & Lauga (2010*a*, 2011) and generalized here to the unsteady feeding problem for periodic Lagrangian strokes.

5.1. *Adjoint optimization framework*

The rescaled nutrient concentration satisfies the advection–diffusion problem, (2.18)–(2.20), and the mean feeding rate, $\langle J\rangle$, is given by

$$\langle J\rangle = -\left\langle \frac{1}{4\pi}\int_{\mathrm{S}} \boldsymbol{n}\cdot\boldsymbol{\nabla} c\,\mathrm{d}S\right\rangle, \tag{5.1}$$

where $\boldsymbol{n}=\boldsymbol{e}_r$ is the outward normal unit vector. Considering a small perturbation, $\delta\boldsymbol{u}=\sum_n \delta\alpha_n(t)\boldsymbol{u}^{(n)}$, in the velocity field, at leading order and for fixed Pe (or equivalently, fixed energetic cost) the resulting modification in mean feeding rate, $\langle \delta J\rangle = \delta\langle J\rangle$, is obtained at leading order as

$$\delta\langle J\rangle = -\left\langle \frac{1}{4\pi}\int_{\mathrm{S}} \frac{\partial}{\partial n}(\delta c)\,\mathrm{d}S\right\rangle, \tag{5.2}$$

where δc is the resulting linear perturbation in the nutrient concentration field c satisfying

$$\varepsilon\left(\frac{\partial}{\partial t}(\delta c)+\boldsymbol{u}\cdot\boldsymbol{\nabla}\delta c\right)-\nabla^2\delta c = -\varepsilon\delta\boldsymbol{u}\cdot\boldsymbol{\nabla} c+\frac{\delta\mathsf{P}}{2\mathsf{P}}\nabla^2 c, \tag{5.3}$$

with Dirichlet boundary conditions, $\delta c=0$, both on the surface of the swimmer and in the far field. The last term in (5.3) guarantees that $Pe=\varepsilon\sqrt{\mathsf{P}}$ is constant and is obtained from $\delta\alpha_n$ and using (2.15) as

$$\delta\mathsf{P} = 2\sum_n \gamma_n\langle\alpha_n\,\delta\alpha_n\rangle. \tag{5.4}$$

From (5.3), the change in mean feeding rate for constant Pe can be computed as

$$\delta\langle J\rangle = \sum_n \langle\tilde{\alpha}_n\,\delta\alpha_n\rangle, \tag{5.5}$$

where

$$\tilde{\alpha}_n(t) = \alpha_n^*(t)-\frac{\gamma_n\alpha_n(t)}{\mathsf{P}}(\langle J\rangle-\mathsf{H}) \tag{5.6}$$

is the gradient of the feeding rate, at constant Pe, with respect to the nth squirming mode amplitude and

$$\alpha_n^*(t) = \frac{\varepsilon}{4\pi}\int_{\Omega_f} g\boldsymbol{\nabla} c\cdot\boldsymbol{u}^{(n)}\,\mathrm{d}\Omega, \quad \mathsf{H} = \left\langle\frac{1}{4\pi}\int_{\Omega_f}\boldsymbol{\nabla} c\cdot\boldsymbol{\nabla} g\,\mathrm{d}\Omega\right\rangle. \tag{5.7}$$

In the above equation, Ω_f is the entire fluid domain, $\boldsymbol{u}^{(n)}$ is the steady velocity field of the nth squirming mode, and the adjoint field, g, satisfies the adjoint advection–diffusion problem

$$\varepsilon\left(\frac{\partial g}{\partial t}+\boldsymbol{u}\cdot\boldsymbol{\nabla} g\right) = -\nabla^2 g, \tag{5.8}$$

together with boundary conditions

$$g\to 0 \quad \text{as } r\to\infty, \tag{5.9}$$

$$g=1 \quad \text{for } r=1. \tag{5.10}$$

A given Lagrangian periodic swimming stroke is defined by the trajectories of the surface material points, $\xi(\mu_0, t)$. The gradient of $\langle J \rangle$ with respect to the stroke, $\xi(\mu_0, t)$, is then the unique function $F[\xi](\mu_0, t)$ such that for any stroke perturbation $\delta\xi$, the resulting modification of $\langle J \rangle$ is

$$\delta\langle J \rangle = \frac{1}{2\pi} \int_0^{2\pi} \int_{\Omega_f} F[\xi](\mu_0, t)\delta\xi(\mu_0, t)\, \mathrm{d}\mu_0\, \mathrm{d}t. \tag{5.11}$$

This gradient can be obtained directly from $\tilde{\alpha}_n(t)$ as

$$F[\xi](\mu_0, t) = \frac{1}{2}\left[\tilde{\alpha}_n L_n'(\xi)\frac{\partial^2 \xi}{\partial \mu_0 \partial t} + \frac{\partial}{\partial t}\left(\tilde{\alpha}_n L_n' \frac{\partial \xi}{\partial \mu_0}\right)\right], \tag{5.12}$$

and then projected onto the subspace of acceptable strokes (periodic trajectories, no displacement at the pole) (Michelin & Lauga 2010*a*). Note that although presented here for the particular case of a spherical swimmer, this optimization framework can easily be generalized to periodic swimming strokes of organisms with arbitrary shapes (Michelin & Lauga 2011).

5.2. *Optimal feeding strokes*

Following Michelin & Lauga (2010*a*) and in order to account for constraints on the stroke kinematics (introduced for example by a finite cilia-length-to-cell-size ratio), an additional constraint is included in the optimization algorithm to limit the maximum amplitude of angular displacements, Θ_{max}, of any surface point during the stroke. This optimization is performed using a steepest-ascent iterative optimization algorithm as described in Michelin & Lauga (2011), and the gradient of the feeding rate with respect to the swimming stroke is computed using the results from previous sections.

Figure 9 shows the optimal strokes obtained for $Pe = 5$ and four increasing values of Θ_{max}. The optimal strokes consist of two different parts: an effective stroke where the surface of the squirmer stretches from front to back, enabling the swimming motion, followed by a recovery stroke where the material points (e.g. cilia tips) accumulated on the back side of the sphere are brought back to their original position with a front-like dynamics, reminiscent of the metachronal waves observed in ciliates. A wave velocity can be defined from the synchronization of the trajectories (Michelin & Lauga 2010*a*). Notice also in figure 9 the phase delay between feeding and swimming predicted theoretically. Imposing tighter bounds on Θ_{max} results in a slower phase velocity of the recovery stroke, in a smaller and steadier swimming velocity, and in a reduced efficiency (table 2). This dichotomy of the optimal stroke and this impact of the maximum displacement Θ_{max} are essentially identical to that observed in the optimal Lagrangian swimming stroke by Michelin & Lauga (2010*a*), for which it was observed that a continuous set of optimal strokes could be obtained for $0 \leqslant \Theta_{max} \leqslant 90°$, approaching asymptotically the optimal steady swimmer when $\Theta_{max} \to 90°$. A similar behaviour is observed on figure 10.

The above conclusions are unchanged when performing the optimization at different values of the Péclet number, as shown in figure 11. For a given constraint on the maximum displacement Θ_{max}, the same strokes are obtained regardless of the value of Pe. These results confirm therefore that the optimal unsteady feeding stroke is essentially the same as the optimal swimming stroke, regardless of the value of the Péclet number. In both cases (swimming or feeding), the optimal Lagrangian stroke can be understood as a periodic approximation of the optimal steady stroke.

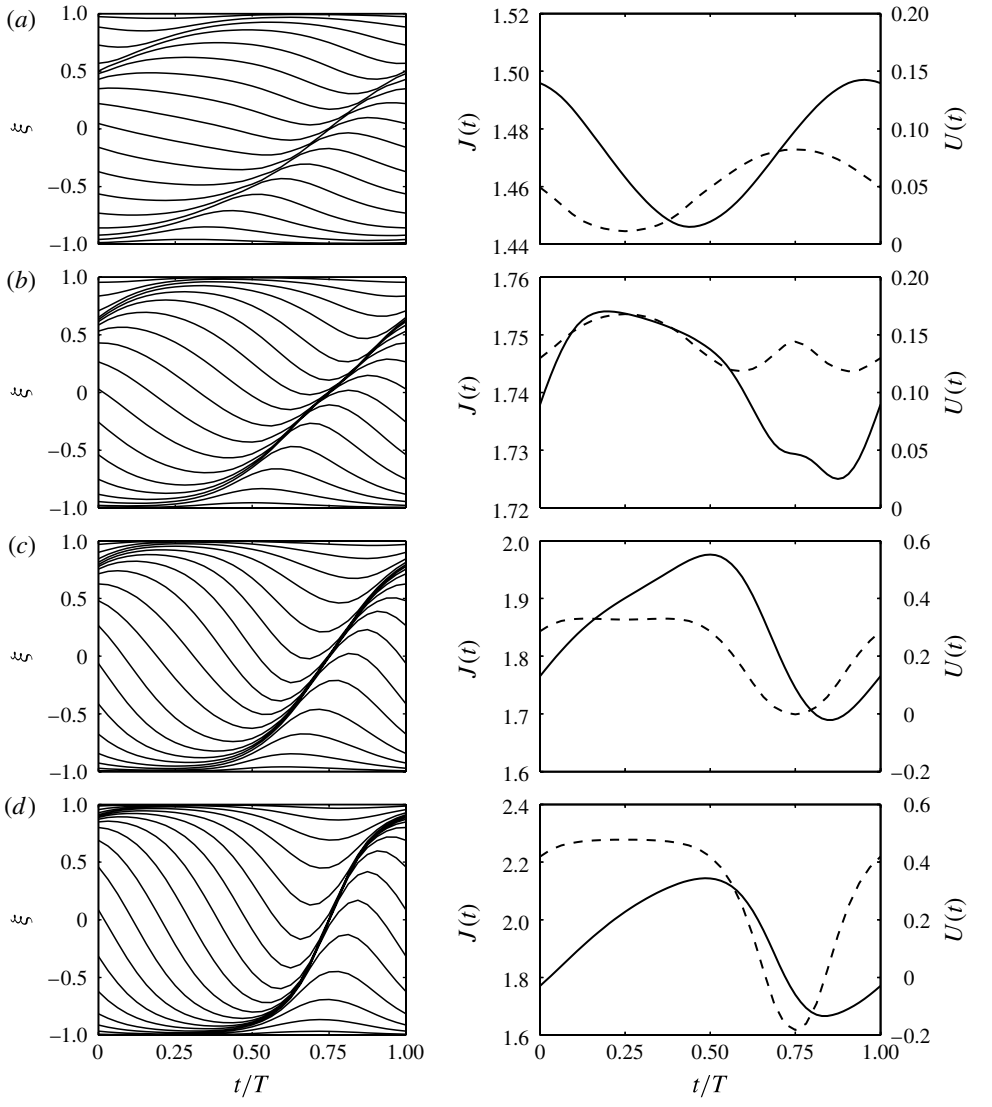

FIGURE 9. Left: Lagrangian trajectories of four optimal feeding strokes, $\xi(t)$, obtained for $Pe = 5$ and a maximum angular stretching of the surface equal to: (*a*) $\Theta_{max} = 12°$; (*b*) $\Theta_{max} = 24°$; (*c*) $\Theta_{max} = 35°$; and (*d*) $\Theta_{max} = 50°$. Right: time-variation for each of these optimal strokes of the instantaneous feeding rate, $J(t)$ (solid), and swimming velocity, $U(t)$ (dashed). The characteristics of these four strokes are summarized in table 2.

6. Conclusions

In this paper we use asymptotic analysis and numerical computations to address the link between swimming and feeding for motile micro-organisms. Using the mathematical model of spherical squirmers acting on the viscous fluid in a time-periodic manner, we first show analytically at low Pe that the mean rate of feeding as well as its fluctuations in time depend only on the swimming modes of the squirmer up to order $Pe^{3/2}$, even when no swimming occurs on average, while the influence of non-swimming modes come in later at order Pe^2. We also demonstrate

	Θ_{max} (deg.)	$\langle J \rangle$	$\langle U \rangle$	η (%)	Pe	ε	Pe_U
(a)	12	1.47	0.048	3.1	5	26.2	1.25
(b)	24	1.74	0.141	10	5	15.9	2.24
(c)	35	1.85	0.221	15	5	12.3	2.73
(d)	50	1.93	0.295	19	5	10.5	3.09

TABLE 2. Characteristics of the optimal feeding strokes obtained computationally for $Pe = 5$ and four maximum angular displacements, Θ_{max}, displayed on figure 9.

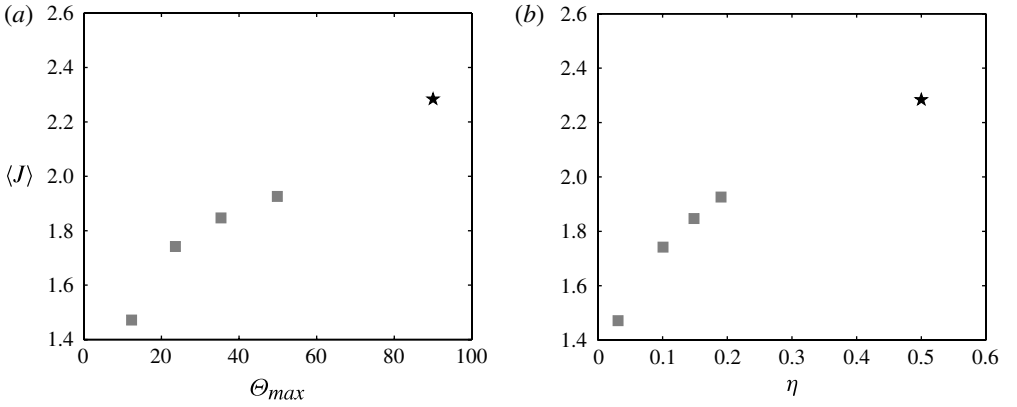

FIGURE 10. (a) Maximum feeding rate, $\langle J \rangle$, as a function of the maximum angular displacement angle, Θ_{max}, in optimal strokes for $Pe = 5$. (b) Maximum feeding rate as a function of swimming efficiency, η, for optimal feeding strokes obtained for $Pe = 5$ and various maximum displacement angles Θ_{max}. The black stars in both figures correspond to the optimal steady stroke (treadmill).

the existence of a phase delay between feeding and swimming of 1/8th of a period. Using three illustrative stokes, we then employ numerical computations to confirm our asymptotic results and further demonstrate the relationship between swimming and feeding. Using adjoint-based optimization we finally determine numerically the optimal unsteady strokes maximizing the feeding rate for a fixed energy budget. The overall optimal is always the steady swimmer. For time-periodic strokes, we find – as in the steady case – that the optimal feeding strokes are equivalent to those optimizing swimming; this result is true for all Péclet numbers even though the value of feeding rate strongly depends on the Péclet number. As for the optimal unsteady swimming problem, optimal feeding strokes are therefore mathematical regularizations of the steady problem (treadmill) of overall maximum swimming and feeding performance.

Clearly the problem studied here is idealized in many ways. The geometry is that of a sphere and the boundary conditions assume perfect nutrient absorption. These simplifications allow us, however, to develop a precise mathematical and computational description of the problem, both for the fluid and for the passive nutrient concentration. It is hoped that the biophysical insight developed in this study will be applicable to a wide range of problems in the realm of micro-organism locomotion, e.g. in bacterial chemotaxis (at low Pe) or the feeding of plankton (at high Pe). One of the main modelling challenges for future work concerns the issue of shape

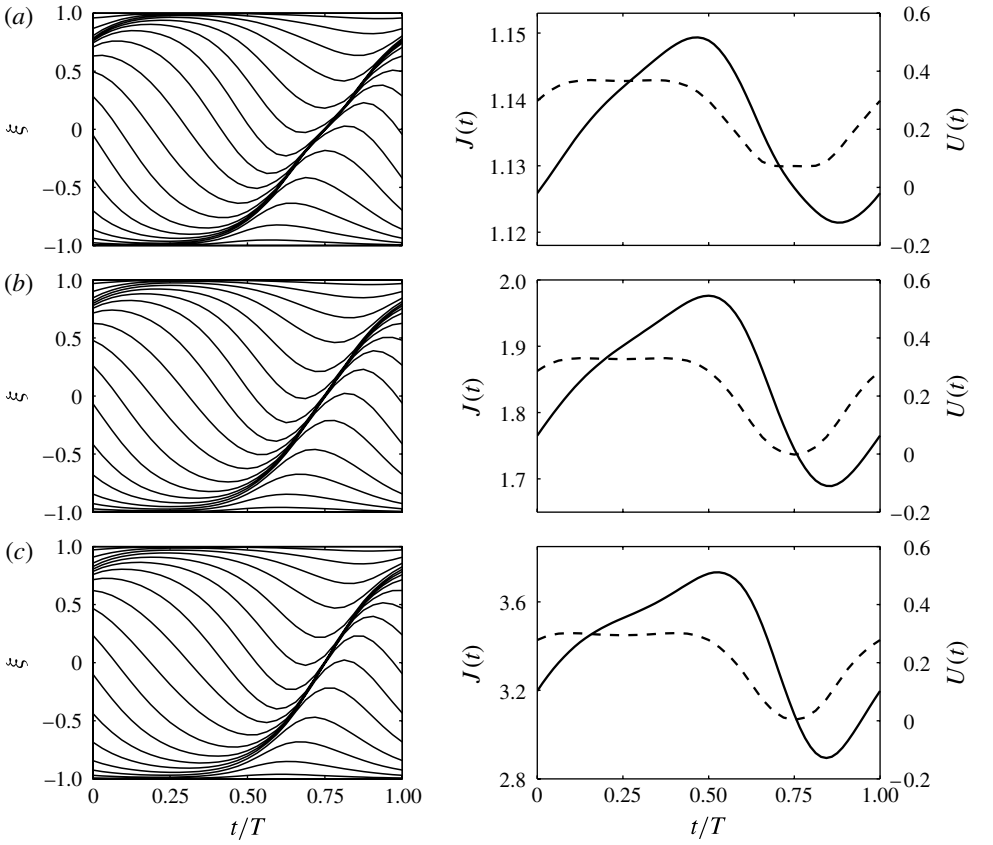

FIGURE 11. Left: Lagrangian trajectories of the optimal time-periodic feeding strokes obtained for $\Theta_{max} = 35^\circ$ and: (*a*) $Pe = 0.5$; (*b*) $Pe = 5$; and (*c*) $Pe = 25$. Right: time-variation for each of these optimal strokes of the instantaneous feeding rate, $J(t)$ (solid), and swimming velocity, $U(t)$ (dashed).

changes. Most motile organisms display a Lagrangian deformation of their shapes. In this paper we have assumed that the deformations (the surface boundary conditions) always act tangentially to the organism surface, allowing the shape to remain that of a sphere. Clearly, normal surface velocities would also need to be considered, and these are precisely the ones leading to changes in shape. The problem would then involve solving for the flow and nutrient concentration around a time-varying boundary. We hope that our study will inspire future work in this direction.

Acknowledgement

This work was supported in part by the US National Science Foundation through grant CBET-0746285.

Appendix A. Unsteady heat/mass transfer around a sphere in Stokes flow

In § 3, the asymptotic expansion of the concentration distribution around a general squirmer and the resulting feeding rate, $J(t)$, were obtained in the limit $Pe \ll 1$. The results obtained in (3.35)–(3.36) also hold for any spherical object moving at

velocity $U(t)$, regardless of whether the sphere is swimming (zero net force) or a rigid sphere actuated by an external force, as we now show.

Considering a generalization of the work of Acrivos & Taylor (1962) to unsteady particle velocity $\alpha_1(t) = U(t)$, the velocity field around the sphere is given by the streamfunction

$$\psi(r,\mu,t) = \frac{\alpha_1(t)(1-\mu^2)}{2}\left(\frac{3r}{2} - r^2 - \frac{1}{2r}\right). \tag{A 1}$$

Following the same approach as in § 3, (3.2) takes the same form but (3.6)–(3.7) become

$$l_1 = -\left(1 - \frac{3}{2r} + \frac{1}{2r^3}\right)\mu\frac{\partial}{\partial r} - \frac{1-\mu^2}{r}\left(1 - \frac{3}{4r} - \frac{1}{4r^3}\right), \tag{A 2}$$

$$l_n = 0 \quad \text{for all } n \geqslant 2. \tag{A 3}$$

In the same way, (3.3)–(3.4) are slightly modified due to the contribution of the Stokeslet in the far field:

$$\text{in the UBL,} \quad \mathsf{D}\,\mathsf{C}_p = \mathrm{i}p\mathsf{C}_p + \varepsilon^{1/2}\sum_{q=-\infty}^{\infty}\alpha_{1,q}\mathsf{L}_1\,\mathsf{C}_{p-q} + \varepsilon\sum_{q=-\infty}^{\infty}\alpha_{1,q}\tilde{\mathsf{L}}_1\,\mathsf{C}_{p-q} + O(\varepsilon^{3/2}); \tag{A 4}$$

$$\text{in the SBL,} \quad \mathscr{D}\mathscr{C}_0 = \alpha_{1,0}\mathscr{L}_1\mathscr{C}_0 + \varepsilon\alpha_{1,0}\tilde{\mathscr{L}}_1\mathscr{C}_0 + O(\varepsilon^2), \tag{A 5}$$

where L_1 and $\mathscr{L}_1$ remain unchanged from (3.8), and

$$\tilde{\mathsf{L}}_1 = \frac{3\mu}{2R}\frac{\partial}{\partial R} + \frac{3(1-\mu^2)}{4R^2}\frac{\partial}{\partial\mu}, \tag{A 6}$$

and $\tilde{\mathscr{L}}_1$ is obtained by replacing R by ρ in the previous equation.

Following the approach of § 3, (3.9)–(3.36) remain unchanged except:

(i) equation (3.19) becomes

$$D\,c_p^2 = \alpha_{1,p}l_1\,c_0^0 = \frac{\mu\alpha_{1,p}}{r^2}\left(1 - \frac{3}{2r} + \frac{1}{2r^3}\right); \tag{A 7}$$

(ii) equation (3.20) becomes

$$c_p^2(r,\mu) = \alpha_{1,p}\mu\left(-\frac{1}{2} + \frac{3}{4r} + \frac{1}{8r^3} - \frac{3}{8r^2}\right) + \sum_{n=1}^{\infty}\gamma_{n,p}L_n(\mu)\left(\frac{1}{r^{n+1}} - r^n\right); \tag{A 8}$$

(iii) equation (3.25) becomes

$$c_p^2 = \frac{\alpha_{1,0}}{2}\left(\frac{1}{r} - 1\right)\delta_{p,0} + \mu\alpha_{1,p}\left(-\frac{1}{2} + \frac{3}{4r} + \frac{1}{8r^3} - \frac{3}{8r^2}\right); \tag{A 9}$$

(iv) and equation (3.31) becomes

$$\frac{1}{R^2}\frac{\mathrm{d}}{\mathrm{d}R}\left(R^2\frac{\mathrm{d}\tilde{\mathsf{C}}_p^3}{\mathrm{d}R}\right) - \mathrm{i}p\tilde{\mathsf{C}}_p^3 = \frac{1}{2}\sum_{q=-\infty}^{\infty}\alpha_{1,p-q}\int_{-1}^{1}\mathsf{L}_1\,\mathsf{C}_p^2\,\mathrm{d}\mu + \frac{1}{2}\sum_{q=-\infty}^{\infty}\alpha_{1,p-q}\int_{-1}^{1}\tilde{\mathsf{L}}_1\,\mathsf{C}_p^1\,\mathrm{d}\mu$$

$$= \frac{1}{3R}\sum_{q}\alpha_{1,p-q}\alpha_{1,q}\mathrm{e}^{-R\sqrt{\mathrm{i}q}}. \tag{A 10}$$

These modifications do not impact on the final result for the nutrient flux at the boundary. The expansion of the feeding rate for an oscillating sphere is therefore identical to that of the squirmer with same swimming velocity up to $O(Pe^{3/2})$ in (3.35)–(3.36). Looking at the corrections in the asymptotic expansion presented above, it appears that any far-field singularity in the velocity field (Stokeslet, etc.) will modify the near-field solution starting at $O(Pe)$ and the unsteady boundary layer starting at $O(Pe^{3/2})$ but that such modifications will only affect the azimuthal fluctuations of the concentration and not its azimuthal average which determines the total feeding rate. Therefore, the asymptotic expansion of the feeding rate remains unchanged for any sphere moving at velocity $\alpha_1(t)$, regardless of the tangential velocity field applied on its surface, and regardless of the total force applied on the sphere.

As a result, (3.35)–(3.36) are a generalization to unsteady motions of the classical result on the heat and mass transfer on a sedimenting sphere (Acrivos & Taylor 1962), and the physical conclusions of § 3 are also valid in the case of a rigid sphere, in particular: (i) the phase delay between the velocity and the mass transfer rate; and (ii) an increase in mass/heat transfer scaling as $Pe^{3/2}$ for a sphere oscillating around a fixed mean position ($\langle U\rangle = 0$).

Appendix B. Definition of the A_{mnp} and B_{mnp} tensors

The coefficients A_{mnp} and B_{mnp} used in (4.3) are defined in terms of the Legendre polynomials as follow:

$$A_{mnp} = \frac{(2p+1)(2n+1)}{2}\int_{-1}^{1} L_m L_n L_p \,\mathrm{d}\mu, \tag{B 1}$$

$$B_{mnp} = \frac{(2p+1)(2n+1)}{2n(n+1)}\int_{-1}^{1} (1-\mu^2) L'_m L'_n L_p \,\mathrm{d}\mu. \tag{B 2}$$

They are easily computed using

$$A_{m0p} = \delta_{mp}, \quad B_{m0p} = 0 \tag{B 3}$$

and the following recursive relations for $n \geqslant 1$:

$$A_{mnp} = \frac{2n+1}{n}\left[-\frac{n-1}{2n-3}A_{m,n-2,p} + \frac{m+1}{2m+1}A_{m+1,n-1,p} + \frac{m}{2m+1}A_{m-1,n-1,p}\right], \tag{B 4}$$

$$B_{mnp} = \frac{2n+1}{n(n+1)}\left[\frac{(n-2)(n-1)}{2n-3}B_{m,n-2,p} + \frac{m(m+1)}{2m+1}\left(A_{m-1,n-1,p} - A_{m+1,n-1,p}\right)\right]. \tag{B 5}$$

REFERENCES

ACRIVOS, A. & TAYLOR, T. D. 1962 Heat and mass transfer from single spheres in Stokes flow. *Phys. Fluids* **4**, 387–394.

BATCHELOR, G. K. 1970 The stress system in a suspension of force-free particles. *J. Fluid Mech.* **41**, 545–570.

BERG, H. C. 1993 *Random Walks in Biology*. Princeton University Press.

BERKE, A. P., TURNER, L., BERG, H. C. & LAUGA, E. 2008 Hydrodynamic attraction of swimming micoorganisms by surfaces. *Phys. Rev. Lett.* **101**, 038102.

BLAKE, J. R. 1971 A spherical envelope approach to ciliary propulsion. *J. Fluid Mech.* **46**, 199–208.

BLAKE, J. R. & SLEIGH, M. A. 1974 Mechanics of ciliary locomotion. *Biol. Rev.* **49**, 85–125.

BRENNEN, C. & WINNET, H. 1977 Fluid mechanics of propulsion by cilia and flagella. *Annu. Rev. Fluid Mech.* **9**, 339–398.

CHILDRESS, S., KOEHL, M. A. R. & MIKSIS, M. 1987 Scanning currents in Stokes flow and the feeding of small organisms. *J. Fluid Mech.* **177**, 407–436.

CRAWFORD, D. W. & PURDIE, D. A. 1992 Evidence for avoidance of flushing from an estuary by a planktonic, phototrophic ciliate. *Mar. Ecol. Prog. Ser.* **79**, 259–265.

DOOSTMOHAMMADI, A., STOCKER, R. & ARDEKANI, A. M. 2012 Low-Reynolds-number swimming at pycnoclines. *Proc. Natl Acad. Sci.* **109**, 3856–3861.

DRESCHER, K., LEPTOS, K. C., TUVAL, I., ISHIKAWA, T., PEDLEY, T. J. & GOLDSTEIN, R. E. 2009 Dancing volvox hydrodynamic bound states of swimming algae. *Phys. Rev. Lett.* **102**, 168101.

EVANS, A. A., ISHIKAWA, T., YAMAGUCHI, T. & LAUGA, E. 2011 Orientational order in concentrated suspensions of spherical microswimmers. *Phys. Fluids* **23**, 111702.

HAMEL, A., FISH, C., COMBETTES, L., DUPUIS-WILLIAMS, P. & BAROUD, C. N. 2011 Transitions between three swimming gaits in Paramecium escape. *Proc. Natl Acad. Sci.* **108**, 7290–7295.

ISHIKAWA, T. & PEDLEY, T. J. 2007 Diffusion of swimming model micro-organisms in a semi-dilute suspension. *J. Fluid Mech.* **588**, 437–462.

ISHIKAWA, T., SIMMONDS, M. P. & PEDLEY, T. J. 2006 Hydrodynamic interaction of two swimming model micro-organisms. *J. Fluid Mech.* **568**, 119–160.

ISHIKAWA, T., SIMMONDS, M. P. & PEDLEY, T. J. 2007 The rheology of a semi-dilute suspension of swimming model micro-organisms. *J. Fluid Mech.* **588**, 399–435.

KESSLER, J. O. 1986 Individual and collective fluid dynamics of swimming cells. *J. Fluid Mech.* **173**, 191–205.

KURTULDU, H., GUASTO, J. S., JOHNSON, K. A. & GOLLUB, J. P. 2011 Enhancement of biomixing by swimming algal cells in two-dimensional films. *Proc. Natl Acad. Sci.* **108**, 10391–10395.

LAUGA, E., DiLUZIO, W. R., WHITESIDES, G. M. & STONE, H. A. 2006 Swimming in circles: motion of bacteria near solid boundaries. *Biophys. J.* **90**, 400–412.

LAUGA, E. & POWERS, T. R. 2009 The hydrodynamics of swimming micro-organisms. *Rep. Prog. Phys.* **72**, 096601.

LEPTOS, K. C., GUASTO, J. S., GOLLUB, J. P., PESCI, A. I. & GOLDSTEIN, R. E. 2009 Dynamics of enhanced tracer diffusion in suspensions of swimming eukaryotic microorganisms. *Phys. Rev. Lett.* **103**, 198103.

LESHANSKY, A. M., KENNETH, O., GAT, O. & AVRON, J. E. 2007 A frictionless microswimmer. *New J. Phys.* **9**, 145.

LIGHTHILL, M. J. 1952 On the squirming motion of nearly spherical deformable bodies through liquids at very small Reynolds numbers. *Commun. Pure Appl. Maths* **5**, 109–118.

LIGHTHILL, J. 1975 *Mathematical Biofluid-Dynamics*. SIAM.

LIN, Z., THIFFEAULT, J.-L. & CHILDRESS, S. 2011 Stirring by squirmers. *J. Fluid Mech.* **669**, 167–177.

MAGAR, V., GOTO, T. & PEDLEY, T. J. 2003 Nutrient uptake by a self-propelled steady squirmer. *Q. J. Appl. Maths* **56**, 65–91.

MAGAR, V. & PEDLEY, T. J. 2005 Average nutrient uptake by a self-propelled unsteady squirmer. *J. Fluid Mech.* **539**, 93–112.

MICHELIN, S. & LAUGA, E. 2010*a* Efficiency optimization and symmetry-breaking in an envelope model for ciliary locomotion. *Phys. Fluids* **22**, 111901.

MICHELIN, S. & LAUGA, E. 2010*b* The long-time dynamics of two hydrodynamically-coupled swimming cells. *Bull. Math. Biol.* **72**, 973–1005.

MICHELIN, S. & LAUGA, E. 2011 Optimal feeding is optimal swimming for all Péclet numbers. *Phys. Fluids* **23** (10).

PEDLEY, T. J. & KESSLER, J. O. 1992 Hydrodynamic phenomena in suspensions of swimming microorganisms. *Annu. Rev. Fluid Mech.* **24**, 313–358.

PURCELL, E. M. 1977 Life at low-Reynolds number. *Am. J. Phys.* **45**, 3–11.

SAINTILLAN, D. & SHELLEY, M. J. 2008*a* Instabilities and pattern formation in active particle suspensions: kinetic theory and continuum simulations. *Phys. Rev. Lett.* **100**, 178103.

SAINTILLAN, D. & SHELLEY, M. J. 2008*b* Instabilities, pattern formation and mixing in active particle suspensions. *Phys. Fluids* **20**, 123304.

SHORT, M. B., SOLARI, C. A., GANGULY, S., POWERS, T. R., KESSLER, J. O. & GOLDSTEIN, R. E. 2006 Flows driven by flagella or multicellular organisms enhance long-range molecular transport. *Proc. Natl Acad. Sci.* **103**, 8315–8319.

SOKOLOV, A., ARANSON, I. S., KESSLER, J. O. & GOLDSTEIN, R. E. 2007 Concentration dependence of the collective dynamics of swimming bacteria. *Phys. Rev. Lett.* **98**, 158102.

SPAGNOLIE, S. & LAUGA, E. 2010 The optimal elastic flagellum. *Phys. Fluids* **22**, 031901.

SUAREZ, S. S. & PACEY, A. A. 2006 Sperm transport in the female reproductive tract. *Hum. Reprod. Update* **12**, 23–37.

TAM, D. & HOSOI, A. E. 2007 Optimal stroke patterns for Purcell's three-link swimmer. *Phys. Rev. Lett.* **98** (6), 068105.

TAM, D. & HOSOI, A. E. 2011*a* Optimal feeding and swimming gaits of biflagellated organisms. *Proc. Natl Acad. Sci.* **108** (3), 1001.

TAM, D. & HOSOI, A. E. 2011*b* Optimal kinematics and morphologies for spermatozoa. *Phys. Rev.* E **83**, 045303.